https://doi.org/10.5194/egusphere-2026-4651
Preprint. Discussion started: 18 August 2026

Evaluating satellite limb measurements of nitrous oxide

Laura N. Saunders[1], Kaley A. Walker[1], Gabriele P. Stiller[2], Piera Raspollini[3], Luis F. Millán[4], Marco Gai[3], Chris D. Boone[5], John Gille[6], Norbert Glatthor[2], Armin Kleinböhl[4], Anne Kleinert[2], Alyn Lambert[4], Donal P. Murtagh[7], Patrick E. Sheese[1], Geoffrey C. Toon[4], and Gerald Wetzel[2]

[1]Department of Physics, University of Toronto, Toronto, Canada
[2]Institute of Meteorology and Climate Research, Karlsruhe Institute of Technology, Karlsruhe, Germany
[3]Istituto di Fisica Applicata "Nello Carrara", Consiglio Nazionale delle Ricerche, Sesto Fiorentino, Italy
[4]Jet Propulsion Laboratory, California Institute of Technology, Pasadena, USA
[5]Department of Chemistry, University of Waterloo, Waterloo, Canada
[6]National Center for Atmospheric Research, Boulder, USA
[7]Department of Space, Earth and Environment, Chalmers University of Technology, Gothenburg, Sweden

Correspondence: Kaley A. Walker (kaley.walker@utoronto.ca)

Abstract. As of the early 2000s, multiple contemporaneous global and vertically resolved nitrous oxide (N_2O) datasets have become available from a suite of limb-viewing satellite instruments. Together, these datasets provide a 23-year and counting continuous N_2O record. Due to its long lifetime, N_2O is a valuable tracer of atmospheric transport, and a reliable long-term record therefore allows the examination of changes in stratospheric circulation as a result of climate change. In order to combine results from different satellite datasets for these purposes, it is necessary to account for their biases, which can be determined through evaluation studies. Here, N_2O measurements in the upper troposphere and lower-to-middle stratosphere (5-40 km) are evaluated from five different satellite limb sounders: ACE-FTS on SCISAT, HIRDLS and MLS on Aura, MIPAS on Envisat, and SMR on Odin. This is done by comparing colocated satellite measurements with each other to determine the instruments' relative biases and by comparing each dataset with independent reference data from balloon-borne instruments. ACE-FTS (v5.2), the two MIPAS datasets (V8), and SMR (v3.0.0) agree within ±5-10%, but HIRDLS (v07) has variable performance depending on the region and time of year. MLS (v5) has a persistent deviation resulting in a low bias of up to 30% in the lower stratosphere at 24 km. This bias is substantially reduced in v6. These findings are corroborated by the comparisons of each satellite instrument with balloon-borne data. This study lays the groundwork for creating a merged and bias-corrected N_2O time series spanning from 2002 to the present using ACE-FTS, MIPAS, SMR, and possibly the MLS v6 dataset.

1 Introduction

Nitrous oxide (N_2O) is primarily emitted through agriculture due to fertilizer use, but it is also a product of fossil fuel combustion, biomass burning, and wastewater management (e.g., Tian et al., 2020). It is photolyzed in the stratosphere to form reactive nitrogen, and with the reduction in chlorine-containing ozone-depleting substances such as chlorofluorocarbons, N_2O is now the dominant anthropogenic gas responsible for ozone depletion (Ravishankara et al., 2009). Its global warming potential (GWP) is 273 on a 100-year timescale (Forster et al., 2021) even with a volume mixing ratio (VMR) more than

https://doi.org/10.5194/egusphere-2026-4651
Preprint. Discussion started: 18 August 2026

five times smaller than that of methane, which has a GWP of 29: approximately 340 ppbv N_2O near the surface as opposed to 1.9 ppmv CH_4 (NOAA, 2026). N_2O has been measured by a variety of instruments from different vantage points. For example, recently, the long-term temporal variability of N_2O from the middle troposphere to the middle stratosphere was evaluated using airborne and balloon-borne measurements between 1987 and 2018 (Krysztofiak et al., 2023).

Space-based limb measurements of N_2O have been available since the late 1970s, beginning with SAMS (Stratospheric and Mesospheric Sounder) aboard the Nimbus 7 satellite (Drummond et al., 1980), which measured infrared emission from January 1979 to June 1983. Its successor, ISAMS (Improved SAMS; Taylor et al., 1993), operated aboard the Upper Atmosphere Research Satellite (UARS) from September 1991 to July 1992. Also aboard UARS was CLAES (Cryogenic Limb Array Etalon Spectrometer; Roche et al., 1993), a mid-infrared emission sounder that took measurements between September 1991 and May 1993. ATMOS (Atmospheric Trace Molecule Spectroscopy, Gunson et al., 1996) and CRISTA (Cryogenic Infrared Spectrometers and Telescopes for the Atmosphere; Riese et al., 1999) both measured N_2O from the Space Shuttle during a series of flights with durations of 1-2 weeks. ATMOS took solar occultation measurements in the infrared on four flights between 1985 and 1994 and CRISTA measured thermal emission on two flights in 1994 and 1997. Solar occultation measurements were also taken by the Improved Limb Atmospheric Spectrometer (ILAS; Kanzawa et al., 2003) aboard the Advanced Earth Observing Satellite (ADEOS) between September 1996 and June 1997 and by its successor, ILAS-II (Ejiri et al., 2006), aboard ADEOS-II between January and October 2003. Since the beginning of the "golden age" of satellite observations in the early 2000s, multiple simultaneous global satellite datasets have become available for N_2O limb measurements. These include SMR (Sub-Millimetre Radiometer; Murtagh et al., 2002), ACE-FTS (Atmospheric Chemistry Experiment Fourier Transform Spectrometer; Bernath et al., 2005), HIRDLS (High Resolution Dynamics Limb Sounder; Gille et al., 2008), MIPAS (Michelson Interferometer for Passive Atmospheric Sounding; Fischer et al., 2008), and Aura-MLS (Microwave Limb Sounder; hereafter, MLS; Waters et al., 2006).

These recent (i.e., since 2002) satellite-based datasets comprise a continuous 23-year global record of N_2O. This record has been used extensively to study processes both in the real atmosphere and within climate models. Due to its long lifetime of about 120 years (Prather et al., 2015), N_2O is an excellent tracer for analyzing stratospheric transport. Some recent examples include using MLS measurements of N_2O to identify transport anomalies in the 2019/2020 Arctic polar vortex (Manney et al., 2022), and trend calculations where N_2O from ACE-FTS was used as a proxy for stratospheric circulation (Dubé et al., 2023, and references therein). Space-based N_2O measurements have also provided important information about processes in the upper atmosphere. Semeniuk et al. (2008) showed with ACE-FTS that N_2O is a signature of energetic electron precipitation, Funke et al. (2008) used MIPAS measurements to study N_2O enhancements during solar proton events in the lower mesosphere, and Sheese et al. (2016) presented the first direct observational evidence, which came from ACE-FTS, of an N_2O source in the lower thermosphere. As a long-lived tracer, N_2O is also useful for age-of-air studies (e.g., Linz et al., 2017; Garny et al., 2024; Dubé et al., 2025, and references therein), which provide observation-based information about changes to the Brewer-Dobson Circulation (BDC). The evolution of the BDC was examined by Minganti et al. (2022) through comparisons of N_2O trends from ACE-FTS with WACCM (Whole Atmosphere Community Climate Model). N_2O measurements from MIPAS and MLS also played a critical role in evaluating a suite of climate models as part of the SPARC (Stratosphere-troposphere Processes

https://doi.org/10.5194/egusphere-2026-4651
Preprint. Discussion started: 18 August 2026

And their Role in Climate) Chemistry-Climate Model Validation activity (SPARC, 2010). They were used to evaluate tropical-extratropical mixing through probability density functions (see also e.g., Douglass et al., 1999; Strahan and Douglass, 2004), the balance of quasi-horizontal transport of young air from low latitudes with descending aged air within the polar vortex, and the effects of descent and mixing in the polar vortex. ACE-FTS measurements of N_2O were used by Kolonjari et al. (2018) to assess mixing and BDC strength in CMAM30-SD, a specified dynamics version of the Canadian Middle Atmosphere Model. These studies, while only representing a subset of the many applications of N_2O measurements, exemplify the utility of the long-term N_2O record.

To maximize the reliability of N_2O studies, it is important to validate the measurements being used through comparisons with other observations. Climatological comparisons between limb-viewing satellite instruments were completed as part of the SPARC Data Initiative (2017), but this was only for the 2006-2009 period and the study was based on only zonal mean data. In this study, as part of the LOLIPOP (LOng-LIved greenhouse gas PrOduct Performances) ESA (European Space Agency) Climate Change Initiative project, a consistent evaluation methodology is applied across profiles from the available satellite-based datasets from the last two and a half decades. The evaluation method used here includes both “intercomparisons” and “validation”. Intercomparisons are comparisons between colocated satellite data, and they are useful because there are near-global colocated measurements between satellite instruments, allowing for a greater scope of the comparison and for more robust comparison statistics. However, with intercomparisons, no single dataset can be used as a reference or “truth” value. This need can be fulfilled through validation, which involves comparing with independent reference data such as balloon measurements so that each satellite instrument’s biases can be understood as well as possible. The satellite datasets to be evaluated and the balloon instruments are described in greater detail in Section 2. Section 3 is a description of the intercomparison methodology and results. The validation methodology and results are presented in Section 4, and a summary and conclusion are provided in Section 5.

2 Datasets used

2.1 Satellite instruments

2.1.1 ACE-FTS

ACE-FTS is a solar occultation instrument on board the Canadian satellite SCISAT and has been measuring up to 30 profiles per day since February 2004 (Bernath et al., 2005). It measures in the mid-infrared from 750-4400 cm^{-1} with a high spectral resolution of 0.02 cm^{-1}. From an orbital inclination of 74°, ACE-FTS samples up to a latitude of 85° in each hemisphere over a three-month period and mostly measures at higher latitudes. The vertical resolution is about 3-4 km as a result of the 1.25 mrad field of view, and the vertical spacing of the measurements is typically 1-6 km. The current version (v5) includes over 70 molecules and isotopologues, along with pressure and temperature, and the retrievals are described in Boone et al. (2023), and references therein. The data are provided on a 1 km grid, and the uncertainty of each measurement is taken to be the statistical fitting error reported from the retrieval. The seasonal median reported uncertainty is small, usually below 5%

https://doi.org/10.5194/egusphere-2026-4651
Preprint. Discussion started: 18 August 2026

except within the Antarctic polar vortex where it is as high as 10%. Version 5.2 was used for this study and while there was recently an update to v5.3, N_2O retrievals were not affected and so the comparisons are still valid for the current version. For v5, N_2O is retrieved from 5-95 km. The data were filtered using the quality flags provided by Sheese et al. (2015): All measurements with a quality flag larger than 0 were removed.

2.1.2 HIRDLS

HIRDLS measured limb emission from aboard the Aura satellite between January 2005 and March 2008 (Gille et al., 2008). From a near-polar (98.2° inclination) sun-synchronous orbit with a 1:30 pm crossing time, HIRDLS covered the 63°S to 80°N range daily, with about 5000 profiles spaced by approximately 100 km. The radiometer had 21 channels, but only one covering 1255.9–1278.5 cm^{-1} was used to measure N_2O. Four channels between 599.8 and 680.8 cm^{-1} measured CO_2 and were used to determine temperature as a function of pressure. During launch, a piece of thermal insulation dislodged and 80-95% of light was blocked from reaching the detectors, reducing the instrument's signal-to-noise ratio. The retrievals are described in Khosravi et al. (2009). The instrument was designed to provide data with 1 km vertical resolution, and the resolution for N_2O has been estimated to be 1.0-1.2 km over the useful vertical range, which is between 100 hPa and 5.1 hPa, or about 15-35 km (Gille and Gray, 2013a). The retrieved VMR, temperature, and altitude are provided on a common pressure grid. The reported uncertainties are the diagonal elements of the covariance matrix, and consist of contributions from measurement noise, forward model error, model parameter error, and smoothing error (Khosravi et al., 2009). The seasonal median uncertainties are large, starting around 10-20% at 15 km depending on the season, and increasing to over 50% at about 30 km. Version 7 was used for this study and as recommended for N_2O, all data with a negative precision were removed and all data outside the 100-5.1 hPa pressure range were excluded (Gille and Gray, 2013a). It is also recommended by the instrument team that, due to the large uncertainties, only zonal mean data be used for scientific applications. However, this assessment is not a scientific application, so individual profiles were considered in order to maintain a consistent comparison methodology across all instruments.

2.1.3 MIPAS

MIPAS was a Fourier transform limb emission spectrometer on board the satellite Envisat, operating from July 2002 to April 2012. Envisat had a 98.55° sun-synchronous orbit with a 10 am equatorial crossing time on its downward leg, completing nearly 15 orbits per day amounting to about 1300 MIPAS profiles per day (Fischer et al., 2008). It measured in five mid-infrared bands between 685 and 2410 cm^{-1}, initially with a spectral resolution of 0.025 cm^{-1}. In March 2004, an interferometer mirror slide malfunction forced a break in measurements until January 2005, when regular operations resumed but the spectral resolution was reduced from 0.025 cm^{-1} to 0.0625 cm^{-1} (von Clarmann et al., 2009). The reduced resolution resulted in a shorter time needed to measure a limb spectrum. The time saved was exploited both to implement a finer vertical sampling of the atmospheric limb and to acquire additional limb scans, about 20% more, within each orbit. The MIPAS data products are split into two periods that are often treated separately: full-resolution (FR, July 2002-March 2004) and reduced-resolution (RR, January 2005-April 2012). MIPAS had daily global coverage from 90°S-90°N and typically measured profiles over tangent heights of 6-70 km. Two MIPAS data products were used in this study: one from the Institut für Meteorologie und

https://doi.org/10.5194/egusphere-2026-4651
Preprint. Discussion started: 18 August 2026

Klimaforschung (IMK) and the Instituto de Astrofísica de Andalucía (IAA), and one from ESA. Both are currently at version 8. The IMK-IAA (hereafter, MIPAS-IMK) retrieval algorithm for the full-resolution period is described by von Clarmann et al. (2003), with the changes made for the reduced-resolution period explained in von Clarmann et al. (2009) and the V8 N_2O retrievals described in Glatthor et al. (2024a). The vertical resolution for MIPAS-IMK, about 3-4 km, is provided in the data files for each individual measurement and is based on the full-width-half-maximum (FWHM) of the averaging kernel row. The measurement uncertainties constitute the total error budget and the seasonal median values are typically about 10-15%, but as large as 40-50% in the polar vortex above about 25 km. All MIPAS-IMK data with a visibility flag of 0 or an averaging kernel diagonal of less than 0.03 were removed. The MIPAS-ESA Level 2 dataset is described in Dinelli et al. (2021), and the retrieval algorithm is presented in Ridolfi et al. (2000), with updates for V8 described in Raspollini et al. (2022). The useful vertical range is from 6 to 60 km for N_2O, and the vertical resolution is provided for each measurement. It is taken as the altitude grid spacing divided by the diagonal values of the averaging kernel, and is typically about 3-4 km below 40 km (Raspollini et al., 2021). The uncertainties provided are the propagated spectral noise error, and the median values are generally lower than 5%, except at higher altitudes (above 35 km) where they increase to about 10% or in the polar vortex above 30 km where they are as large as 40%. The data files include a quality flag, and all profiles with a quality flag not equal to zero were removed.

2.1.4 Aura-MLS

MLS is a limb emission sounder that was launched in July 2004 on Aura and began taking measurements in August (Waters et al., 2006). It measures in five spectral regions between 118 GHz and 2.5 THz (about 4-83 cm^{-1}). MLS covers up to 82° in both hemispheres. It scans the limb every 24.7 s, resulting in around 3500 profiles per day which are output on a uniform pressure grid. The vertical resolution of the measurements is determined by the FWHM of the equatorial averaging kernel at each pressure level and is typically between 5 and 8 km (Livesey et al., 2022). Kernels at other latitudes are similar. The original measurement band for MLS N_2O was in the 640 GHz region (Lambert et al., 2007) and was operated from launch until its failure in 2013. However, to provide a continuous MLS N_2O data product over the entire mission, the MLS team switched to a band in the 190 GHz region. Details about the version 5 (v5) product, which was used for this study, discussed in Livesey et al. (2022). A new version (v6) was recently released (Livesey et al., 2026), with an improved N_2O 190 GHz retrieval that substantially reduces the lower-stratospheric biases present in v5. Since v6 was released after this analysis was completed, all results presented here are based on the v5 datset, with a brief update including v6 presented in Section 3.3. As with HIRDLS, the MLS VMR and temperature are reported on a uniform pressure grid, and the reported uncertainty corresponds to the 1σ-precision of the data. The median uncertainties are around 5-10% but increase to over 50% above about 30 km, or about 22 km in the polar vortex. The data are flagged with a number of diagnostic values to describe measurement quality. As recommended by Livesey et al. (2022), all data with an odd status number, a quality value less than 0.8, a convergence value greater than 2, or a precision less than 0 were removed. Only measurements from 100-0.46 hPa (about 15-55 km) are recommended for scientific use, so measurements outside of this range were excluded.

https://doi.org/10.5194/egusphere-2026-4651
Preprint. Discussion started: 18 August 2026

Table 1. Details of measurements from GLORIA-B. The altitudes refer to the altitude range of available measurements and not the balloon altitude. For descriptions of each quantity, see text.

Location	Mean latitude	Mean date/time	Altitude range [km]	Coincidences ACE-FTS	HIRDLS	MIPAS-ESA	MIPAS-IMK	MLS	SMR
Kiruna, 68°N	67.38°N	21 Aug 2021/23h	10-36	80	0	0	0	1141	1
Timmins, 46°N	51.13°N	24 Aug 2022/2h	7-33	49	0	0	0	1213	4

2.1.5 SMR

SMR measures thermal emission from aboard the Odin satellite, which was launched into a 97.8°-inclination sun-synchronous near-terminator orbit in February 2001 (Murtagh et al., 2002). Its spectral range is 486-581 GHz (about 16-20 cm^{-1}) and it has an effective spectral resolution of about 2 MHz. The data cover up to 82° in each hemisphere except during polar spring, when the instrument is pointed at higher latitudes for short periods. Each target gas is only measured on every third observation day, so at 65 scans per orbit in stratospheric mode this amounts to about 900 N_2O profiles every three days that are provided on a uniform pressure grid. The profiles extend from about 12-70 km. The retrieval method for N_2O is described in Urban et al. (2005), and version 3.0.0 was used for this study. The reported uncertainties are the total retrieval error, which corresponds to the error due to thermal noise and all interfering smoothing errors. The median uncertainty is around 5% below 27 km, and closer to 10% above this. The averaging kernel for each profile is also provided, and the FWHM can be used to estimate the vertical resolution, which ranges from about 3-6 km for measurements below 40 km in altitude. No additional filtering was performed for the SMR data.

2.2 Balloon instruments

2.2.1 GLORIA-B

GLORIA (Gimballed Limb Observer for Radiance Imaging of the Atmosphere) is an imaging Fourier transform spectrometer that measures thermal emission in the 780-1400 cm^{-1} range (Friedl-Vallon et al., 2014). Typically, it measures a variety of gases including N_2O at a spectral resolution of 0.0625 cm^{-1}. The aircraft version of GLORIA is mounted on a gimbal, which allows for easy movement of the instrument and therefore measurement of multiple limb directions. GLORIA-B is the balloon-borne version (Wetzel et al., 2025) of the instrument, and it has flown during two campaigns that are described in Table 1. The altitudes provided refer to the altitude range of available measurements and not the balloon altitude. The table also contains the number of coincident N_2O profiles found between each satellite instrument and each GLORIA-B profile. The methodology for finding these coincidences is described below, in Section 4.1.

For GLORIA-B, the mean of the profiles taken over the course of each flight was used for comparison, so the mean latitude of these profiles is provided in addition to the nominal latitude of the launch site. The Kiruna flight occurred between 21 August

https://doi.org/10.5194/egusphere-2026-4651
Preprint. Discussion started: 18 August 2026

Table 2. Details of measurements from MIPAS-B. The altitudes refer to the altitude range of available measurements and not the balloon altitude.

Location	Date	Sequence	Altitude range [km]	Coincidences ACE-FTS	HIRDLS	MIPAS-ESA	MIPAS-IMK	MLS	SMR
Kiruna, 68°N	12 Feb 2002	01	12-32	0	0	0	0	0	58
Aire-sur-l'Adour, 44°N	24 Sep 2002	n3	9-38	0	0	374	378	0	0
Kiruna, 68°N	20 Mar 2003	n3a	11-31	0	0	209	223	0	72
Teresina, 5°S	14 Jun 2005	12	12-33	0	2235	131	133	1204	55
Teresina, 5°S	6 Jun 2008	03e	16-38	0	0	464	462	1171	131
Kiruna, 68°N	11 Mar 2009	09a	10-33	77	0	347	397	1002	163
Kiruna, 68°N	24 Jan 2010	07d	9-34	193	0	141	195	682	0
Kiruna, 68°N	31 Mar 2011	06	9-35	44	0	223	262	0	83
Timmins, 46°N	7 Sep 2014	05a	14-36	45	0	0	0	1213	93
Timmins, 46°N	7 Sep 2014	05b	14-36	42	0	0	0	1220	92

2021 at 17 h and 22 August 2021 at 6 h, and the Timmins flight occurred between 23 August 2022 at 20 h and 24 August 2022 at 9 h. For both mean profiles, the mean latitude and mean time were used to find coincident measurements.

2.2.2 MIPAS-B

MIPAS-B is the balloon-borne precursor to the MIPAS satellite instrument (Friedl-Vallon et al., 2004, and references therein). It measures in the spectral range of 714-2500 cm^{-1} with a resolution of 0.0345 cm^{-1}. Compared to the satellite instrument, it has a superior line-of-sight stabilization system and noise-equivalent spectral radiance, allowing the tangent altitude to be known to 50 m at the 1σ confidence level (Wetzel et al., 2010). The MIPAS-B sequences (i.e., profiles) used for this study are listed in Table 2, which is similar to Table 1 but contains a column for the "sequence number". The 2014 sequences contain more spectra than the others as they were taken for studying diurnal cycles. As such, two sequences were used, 05a and 05b, as they contain the most spectra. These were treated as two separate profiles throughout this analysis; that is, they were not averaged together prior to making comparisons.

2.2.3 MkIV

MkIV is a Fourier transform infrared spectrometer that performs measurements in solar occultation geometry in the mid-infrared between 650 and 5450 cm^{-1} with 0.006 cm^{-1} resolution (Toon, 1991). The wide spectral range allows the simultaneous measurement of over 30 gases, including N_2O. The instrument has taken measurements from high-altitude balloons over the course of 28 flights since 1989, 18 of which overlap with the measurement periods of the satellites being evaluated in this study. These 18 flights are described in Table 3. The flights consisting of both a sunrise and a sunset profile are treated separately in

https://doi.org/10.5194/egusphere-2026-4651
Preprint. Discussion started: 18 August 2026

Table 3. Details of measurements from MkIV. The altitudes refer to the altitude range of available measurements and not the balloon altitude.

Location	Date	Event	Altitude range [km]	Coincidences ACE-FTS	HIRDLS	MIPAS-ESA	MIPAS-IMK	MLS	SMR
Kiruna, 68°N	16 Dec 2002	Sunrise	13-30	0	0	240	274	0	66
Kiruna, 68°N	1 Apr 2003	Sunrise	11-32	0	0	140	153	0	57
Ft. Sumner, 34°N	19 Sep 2003	Sunset	5-37	0	0	219	227	0	53
Ft. Sumner, 34°N	23 Sep 2004	Sunset	10-37	0	0	0	0	1217	102
Ft. Sumner, 34°N	20 Sep 2005	Sunset	11-38	11	2183	0	0	1199	92
Ft. Sumner, 34°N	21 Sep 2005	Sunrise	15-30	14	2185	0	0	1193	89
Kiruna, 68°N	22 Feb 2007	Ascent	25-34	40	948	133	143	518	37
Ft. Sumner, 34°N	22 Sep 2007	Sunset	13-38	8	1935	97	98	1208	132
Ft. Sumner, 34°N	23 Sep 2007	Sunrise	11-38	7	1950	71	73	1215	125
Ft. Sumner, 34°N	23 Sep 2011	Sunset	5-39	6	0	322	326	1206	163
Ft. Sumner, 34°N	24 Sep 2011	Sunrise	14-40	7	0	353	357	1209	164
Ft. Sumner, 34°N	13 Sep 2014	Sunset	6-39	1	0	0	0	1206	82
Ft. Sumner, 34°N	14 Sep 2014	Sunrise	6-40	3	0	0	0	1206	77
Ft. Sumner, 34°N	27 Sep 2016	Sunset	12-40	15	0	0	0	1220	12
Ft. Sumner, 34°N	7 Oct 2019	Sunset	7-39	19	0	0	0	1209	0
Ft. Sumner, 34°N	25 Sep 2021	Sunset	14-39	3	0	0	0	1032	37
Ft. Sumner, 34°N	26 Sep 2021	Sunrise	9-41	3	0	0	0	1203	35
Ft. Sumner, 34°N	27 Sep 2023	Sunset	11-40	9	0	0	0	1204	0

the table and throughout the analysis. They are listed as profiles measured on consecutive days. One profile, in Kiruna on 22 February 2007, was measured during the balloon's ascent.

3 Intercomparison of satellite profiles

3.1 Intercomparison methodology

The satellite instruments being compared have different sampling patterns due to their individual orbits and measurement frequencies. Because of this and the different time periods during which they operated, it is important to reduce sampling bias by finding coincident measurements between datasets prior to making any comparisons. It is not reasonable to search for coincidences between six datasets simultaneously; it is more practical to search for colocated measurements between pairs of instruments. The process for finding colocated measurements between a "tested" and a "comparison" dataset is described below.

https://doi.org/10.5194/egusphere-2026-4651
Preprint. Discussion started: 18 August 2026

The datasets were first harmonized into the same format and interpolated onto the same 1 km altitude grid. The N_2O vertical distribution is generally smooth and does not have vertical structures on the scale of the instruments' vertical resolutions (i.e., up to about 6 km), therefore no smoothing was done. The harmonized files are described in the Supplementary Information. For each tested profile, all comparison profiles taken within 6 hr and 300 km were considered. The coincidence criteria were chosen to yield enough coincidences to reduce noise in the average of coincident profiles without sacrificing the quality of the comparisons. Using a stricter coincidence criterion of 3 hr did not significantly improve the comparisons and sacrificed a large number of coincidences, and using less strict criteria of 12 hr or 1000 km resulted in worse comparisons (i.e., larger inter-instrument differences) without substantially reducing noise. When there were multiple comparison profiles available, the closest one in horizontal space with valid data that had not already been used was taken to be the coincident profile.

Four types of figures are used to present the intercomparisons between 8 and 40 km. The first two are profile comparisons, plotted against altitude and organized into one row per three-month period (December-January-February, DJF; March-April-May, MAM; June-July-August, JJA; September-October-November, SON) and one column per latitude band. In the first type of figure, the median N_2O profiles are used to determine whether an instrument has any unusual features that persist across different times of year and locations. The median was used instead of the mean because it is less sensitive to outliers. As an estimate of the variability within each dataset, the median absolute deviations (MADs) are also shown, as dashed lines. In the comparisons shown below, SMR is used as the tested dataset because it has the most temporal overlap with the other instruments and a high measurement density, so more coincidences can be found. The SMR medians and MADs are made up of all profiles for the given time of year and latitude band. For other instruments, that is the comparison instruments, the medians are made up of profiles that are coincident with SMR. It should be noted that the profiles from the comparison instruments should not be compared with each other as they represent different subsections of the SMR measurement times and locations.

The second type of figure, the other profile comparisons, are the median relative differences between SMR and each comparison instrument, where a positive value indicates a positive bias in SMR or a negative bias in the comparison instrument. These figures can appear to be inconsistent with the profile comparisons discussed above for two reasons. First, the bias profiles show the median of the differences rather than the difference of the medians, which can noticeably differ for an ensemble with high variability. Second, the differences are calculated between the coincident profiles only, while Figure 1 shows all profiles of the tested instrument. These two datasets can differ significantly. Due to the differences in sampling, the results for the comparison instruments should not be directly compared with one another using either of these profile figures; only the comparisons with SMR are between equivalent samples. The figures showing the VMR and relative difference profiles using each of the other instruments as the tested dataset can be found in the Supplementary Information.

In the third type of figure, normalized probability density functions (PDFs) are used to investigate the distribution of individual measurements at four altitudes spaced by 5 km: 18 km, 23 km, 28 km, and 33 km. This range of altitudes in the lower-to-middle stratosphere was chosen as it includes the region with the strongest vertical N_2O gradient; the VMR is very low above 33 km and nearly constant below 18 km. PDFs can indicate whether differences in the median profiles are due to outliers in a particular dataset or a systematic bias in the measurements. Each row corresponds to one altitude and each column shows the comparison between a tested instrument (coloured based on altitude) and one other comparison dataset (grey). SMR

https://doi.org/10.5194/egusphere-2026-4651
Preprint. Discussion started: 18 August 2026

is once again used as the tested instrument and the remaining PDFs testing the other datasets are shown in the Supplementary Information.

For ease of interpretation, the intercomparisons are summarized in grid plots, which are the fourth and final type of figure. Each figure shows the comparisons for one instrument (i.e., the tested instrument) during each season, one per quadrant, and every box corresponds to one altitude (one of those used for the PDFs, by row) and one comparison instrument (by column). The box colour corresponds to the median relative bias between the two datasets for that season, with red indicating a positive bias in the tested dataset and blue indicating a negative bias. The median absolute differences (in ppbv) and median relative differences are shown in text on each box. The goal of these figures is to make it easier to see if any instrument has a consistent bias across comparisons with other satellite instruments by altitude or season. The summaries for every instrument, not just SMR, are included in the main text.

3.2 Intercomparison results

The median N_2O and MAD profiles as described in Section 3.1 are presented in Figure 1. In general, the profiles and variabilities agree quite well, but there are some noticeable outliers. MLS v5 has a clear low bias from about 20-27 km, due to a deviation in the profile, in most regions except for the polar vortex (60-90°N in DJF; 60-90°S in JJA and SON). In some regions, especially the tropics and midlatitudes, the HIRDLS MAD is larger than for the other instruments. This is explored further below with the PDFs. Some instruments, in particular HIRDLS, MLS, and SMR also have unphysical features at lower altitudes, usually below about 18 km in the upper troposphere-lower stratosphere (UTLS). These are accompanied by higher variability, which for HIRDLS is likely caused by the difficulty in obtaining measurements near the cloud top. The largest deviations between SMR and the comparison instruments were found during the breakup of the polar vortex (60-90°N in MAM and 60-90°S in SON). This could be explained by a large local variability that might not be fully accounted for by the coincidence criteria chosen, as these criteria do not take the location of the vortex into account. The instruments agree better with SMR in the Antarctic than the Arctic because the polar vortex is more consistent there from year to year, which reduces the effects of this particular sampling issue. In these regions of larger disagreement, the MAD is also larger than in other regions as expected due to the greater interannual variability.

The median relative differences between SMR and each other instrument are shown in Figure 2. The agreement between SMR and each of ACE-FTS, and MIPAS (-IMK and -ESA, during both measurement periods) is very good; the differences are mostly within 10% outside of the polar vortex. It is worth noting that the magnitudes of the differences between SMR and the full-resolution MIPAS datasets are generally slightly smaller (by a few percent) than between SMR and the reduced-resolution MIPAS datasets. This is especially true below about 18 km where there is a stronger deviation between SMR and the full-resolution MIPAS data. Within the Antarctic polar vortex, the differences reach over 40% but this is due to the very low N_2O VMRs that result from strong subsidence. In the Arctic polar vortex, the differences are still within 25% except for with MIPAS-ESA where the SMR reaches a high bias of 30% at 30 km. The mid-stratospheric deviation in the MLS v5 profile is even more obvious here; SMR has a high bias of +15-25% relative to MLS at 24 km in all regions except the Antarctic during SON, where the bias is even larger: 35% at 24 km and over 40% at 23 km. Additionally, MLS has a systematic high bias relative to SMR above about 30 km that goes up to about 40%. The SMR bias relative to HIRDLS is also more apparent here; the median difference profile is consistently S-shaped but centred at different values. In some regions, the biases are mostly positive (e.g., 30-60°S in JJA) and in others, the bias is positive at lower altitudes (below 25-28 km) and negative at higher altitudes (e.g., 30-60°S during DJF, MAM, and SON). The width and magnitude of each curve in the S-shape also varies by region; the differences are generally smaller at lower latitudes. SMR also has a systematic low bias of up to about 12% below 20 km and a systematic high bias of up to about 25% above 35 km. Relative differences at these high altitudes will tend to be larger due to the small VMRs (i.e., less than 50 ppbv).

The PDF comparisons between SMR and each other dataset (with the MIPAS full-resolution and reduced-resolution periods separated) are shown in Figure 3. Peculiarities in the HIRDLS PDFs relative to the others are expected because they use individual measurements rather than zonal means (see Section 2.1.2). At 18 km, the agreement is very good with ACE-FTS, MIPAS-ESA, and MLS. The HIRDLS low bias and the MIPAS-IMK high bias are both evident, and the larger MIPAS-IMK peak is flatter than that for SMR, indicating higher variability. The high-VMR side of the larger peak for SMR appears to be slightly steeper than for ACE-FTS, HIRDLS, MIPAS-ESA (reduced-resolution), and MIPAS-IMK (both measurement periods). At 23 km, SMR agrees remarkably well with ACE-FTS and both MIPAS datasets in terms of peak locations, widths, and heights. There is greater disagreement with HIRDLS and MLS, but the profile comparisons showed that these instruments are the outliers at this altitude. This is close to where the MLS v5 deviation causes the largest differences. This appears to be a systematic difference because the centres of the two peaks at larger VMRs (e.g., near 175 ppbv and 275 ppbv for SMR) are shifted low in MLS by about 50 ppbv relative to SMR, but the peak widths and heights are consistent between the two datasets. The HIRDLS distribution, however, is notably different from the SMR distribution: the two peaks at larger VMRs are further apart for HIRDLS and are not as sharp, which is consistent with HIRDLS having larger variability than the other datasets. The same is mostly true at 28 km, but agreement with MLS is much better because this is above the deviation. The high-VMR side of the rightmost peak for SMR is again slightly steeper than for HIRDLS and the two MIPAS reduced-resolution datasets. The SMR PDFs agree very well with those from all other instruments at 33 km except HIRDLS, which is missing a very small second peak just below 150 ppbv. ACE-FTS does not show this peak either, but nor do the SMR measurements that are coincident with the ACE-FTS measurement grid. The PDFs at this altitude in particular demonstrate the importance of comparing coincident measurements, as PDFs covering different regions of the globe will not have the same features.

Figure 4 summarizes the median ACE-FTS N_2O biases. Approximately three quarters of the boxes have small negative biases, but otherwise there is no pattern or clustering that stands out. Below 33 km, the relative biases are mostly within 5%, and with the exception of MLS at 23 km, all are within 10%. The relative biases at 33 km are larger and negative, up to -23%, due to the small VMRs at this altitude.

The HIRDLS biases are summarized in Figure 5. They are more frequently negative (46 boxes) than positive (34 boxes) and the sign of the bias is loosely clustered by altitude. The biases are almost all negative at lower altitudes (18 km and 23 km) during JJA and SON; the bias relative to MLS is positive at 23 km but this is due to the deviation in the MLS dataset. The biases are all negative at 28 km during JJA and mostly all negative during DJF except for compared to ACE-FTS, which also has a negative bias at this altitude when compared with the other three instruments. During MAM, the biases are all positive but

https://doi.org/10.5194/egusphere-2026-4651
Preprint. Discussion started: 18 August 2026

during SON, the sign changes depending on the reference instrument. At 33 km, the biases are positive during DJF and MAM, mostly positive during SON (except compared to MLS), and varying during JJA. This modest altitude clustering is consistent with the S-shape of the bias profiles seen in Figure 2.

The median full-resolution MIPAS-ESA biases are shown in Figure 6. The comparisons with ACE-FTS are included for completeness, but since these are based on just about one month of data (February to March 2004), only the comparisons with MIPAS-IMK and SMR are discussed here. Of the 32 boxes, 25 show negative biases and they are generally quite small: all but four are within −5%. Aside from this, there are no clear issues with the dataset based on these intercomparisons. Figure 7 shows the biases for the reduced-resolution period. Unlike the full-resolution period, they skew positive: 63 of 80 boxes show a positive bias. There is a negative bias relative to MIPAS-IMK at 18 km during all four seasons and aside from slight negative biases relative to HIRDLS at 18 and 28 km during MAM, the rest of the negative biases occur at 33 km. Except for the MLS comparisons, the biases are all within 10%, with most (61 boxes) within 5%. Based on these intercomparisons, both periods of the MIPAS-ESA N_2O dataset are generally reliable.

Figure 8 shows the biases for the full-resolution period of the MIPAS-IMK dataset. As with full-resolution MIPAS-ESA, the comparisons with ACE-FTS are not discussed. The 32 boxes are evenly split between positive and negative biases, with two patterns emerging. The first is a negative bias at 23 km compared to both other datasets during DJF, JJA, and SON, and the other is a positive bias at 18 km during MAM, JJA, and SON. All relative differences are within 10%, and all but 7 boxes have relative differences within 5%. The larger differences are found at 18 km and at 33 km. The latter is not surprising due to the smaller VMRs, but the former is indicative of a greater bias at lower altitudes than in the middle stratosphere. Similarly to reduced-resolution MIPAS-ESA, most of the reduced-resolution MIPAS-IMK absolute differences relative to other instruments, shown in Figure 9, are positive, though the skew is less pronounced than for MIPAS-ESA: 51 out of 80 boxes have positive differences. There is a unanimous positive bias at 18 km of 3-11%, and a nearly unanimous negative bias, except compared to ACE-FTS, at 33 km of up to 14%. Aside from the MLS comparisons at 23 km, the relative differences at 23 km and 28 km are all within 10%, with only 4 of 36 boxes having relative differences above 5%. The MIPAS-IMK intercomparisons for both measurement periods show that both datasets are reliable but have a minor positive bias at 18 km and an even smaller negative bias at 33 km.

The median MLS biases are summarized in Figure 10. There is clearly a negative bias at 23 km (around 32 hPa) of 9-27% when compared with all instruments. This is due to the deviation in the N_2O profile that is present throughout the entire dataset, except in the polar vortex. At 18 km and 28 km, the biases are a mix of positive and negative (16 and 24 boxes, respectively), but the biases are all positive at 33 km aside from the HIRDLS comparison. Apart from at 23 km, the biases are mostly within 10%; only 6 boxes at 33 km have larger biases that are as great as 24%. It should be noted that while MLS v5 was evaluated as part of the LOLIPOP project, MLS v6 has since been released and this deviation is greatly reduced. A brief comparison between each of v5 and v6 with SMR is shown in the section that follows.

Finally, Figure 11 shows the summary of median SMR biases, which are approximately half positive (41 boxes) and half negative (38 boxes), with one box having a difference of exactly zero. Below 33 km, the differences are within 5% aside from 11 boxes of the 60, and these include the 4 representing MLS comparisons at 23 km. At 33 km, the differences are still within

https://doi.org/10.5194/egusphere-2026-4651
Preprint. Discussion started: 18 August 2026

12%, which is very good for such a small concentration. Overall, SMR appears to perform very well compared to the other instruments; this is another reason that it was chosen as the tested instrument to highlight earlier in this section.

3.3 MLS v6

The profile analyses were repeated using MLS v6 in addition to MLS v5 as comparison instruments. For simplicity, as above, the medians are based on profiles that are coincident with SMR. The VMRs and MADs are shown in Figure 12, and the agreement between MLS v6 and SMR is much better than between MLS v5 and SMR. The large deviation at 23 km is no longer present except in the Antarctic during SON. The MAD has not changed significantly between versions. The median relative differences between SMR and each of the MLS versions are shown in Figure 13. The consistent positive bias at 23 km is much smaller, closer to 5-10% instead of up to 25%. The biases above 25 km are generally of different signs outside the tropics; compared to MLS v5, the SMR bias is mostly negative and compared to MLS v6, it is mostly positive. The magnitude of the relative differences at these altitudes is similar between the versions or slightly smaller for MLS v6.

4 Validation of satellite profiles with balloon data

4.1 Validation methodology

Here, zonal means of satellite profiles coincident with a balloon-based reference profile were evaluated. The goal of this methodology was to find coincidence criteria between the satellite and reference data to balance the competing needs of obtaining a statistically significant dataset while limiting the risk of introducing biases. While it would be ideal to use the same coincidence criteria across all satellite datasets, this was impractical given the difference in data density between ACE-FTS and the other instruments. With long-lived tracers such as N_2O, however, changing the criterion for time coincidence has minimal impact on the results and can allow for many more statistical comparisons. Therefore, only the time coincidence criterion was changed for the ACE-FTS comparisons.

Several spatial and temporal criteria were tested and it was found that for HIRDLS, MIPAS, and MLS, the criteria had little impact on the agreement with the balloon profiles, so the main criteria were selected to allow for suitable statistics from SMR, which is a slightly lower-density sampler than the others (aside from ACE-FTS). It was found that matching profiles within 72 hr and 5° latitude yielded more coincidences without sacrificing quality of the comparisons. The latitude criterion was applied at each altitude separately. For ACE-FTS, a time coincidence criterion of 720 hrs (about one month) was used. An additional criterion was introduced for balloon profiles north of 60°N: Colocated measurements must be in the same region with respect to the polar vortex. The vortex edge was identified using scaled potential vorticity (sPV) values provided as part of the Jet Propulsion Laboratory (JPL) Derived Meteorological Products (Manney et al., 2007, 2011; Millán et al., 2023), which are based on the MERRA-2 (Modern Era Retrospective analysis for Research and Applications; Gelaro et al., 2017) reanalysis. Measurements with a corresponding sPV less than $1.2 \times 10^{-4} s^{-1}$ were categorized as outside the vortex, while those with an sPV greater than $1.6 \times 10^{-4} s^{-1}$ were categorized as inside the vortex. Between these two values, measurements

https://doi.org/10.5194/egusphere-2026-4651
Preprint. Discussion started: 18 August 2026

were categorized as within the vortex edge itself. This criterion was applied at each altitude separately. Negative sPV values were not a concern, as all extratropical balloon profiles were taken in the northern hemisphere. The polar vortex criterion is not commonly used for satellite-balloon comparisons, but here it was found to drastically improve agreement for flights launched from Kiruna at 68°N. In addition, the combination of the 5° latitude and vortex coincidence criteria yielded more coincidences as well as better agreement between datasets than using a relatively small distance criterion, such as 300 km. The number of coincidences changed with altitude due to the latitude and, if applicable, vortex criteria. The number reported in Tables 1 through 3 therefore indicates the maximum number of coincidences for each balloon profile. In addition, the number includes only satellite measurements that were retained after filtering, which is why MIPAS-ESA and MIPAS-IMK do not have exactly the same number of coincidences.

For each balloon flight, the measured N_2O VMRs and estimated uncertainties were linearly interpolated onto the harmonized satellite dataset altitude grid. Since the vertical sampling and resolutions of the limb profile measurements and balloon remote-sensing observations are quite similar (2-5 km, typically), these comparisons use the native profiles without accounting for the averaging kernels. Then, the coincident profiles from each satellite dataset were averaged together and compared with the interpolated balloon profile. The relative difference was calculated as the mean of the relative differences between each coincident satellite profile and the balloon profile, with the balloon profile used as the reference. With nearly 40 balloon flights and 6 satellite datasets, it is impractical to show each direct comparison. Instead, as in Wetzel et al. (2022) where MIPAS-ESA was compared with MIPAS-B, the mean comparisons for flights within the Arctic (60-90°N), the midlatitudes (30-60°N), and the tropics (south of 30°N) are presented, and the figures are separated by balloon instrument. For these figures, the means, standard deviations, uncertainties, and mean relative differences were simply averaged together within each region. This was done in order to weight each flight equally without regard for the number of coincidences available. The goal was to present the "mean comparison" of individual flights within each region rather than an overall comparison of mean measurements. The left panels show the mean of all balloon flights, and the mean of their uncertainties, for the relevant instrument within the region as well as the mean of the mean satellite profiles. The right panels show the mean of the relative differences described above. Note that they do not show the relative difference between the mean VMRs in the left panel, so there can appear to be discrepancies especially where VMRs are small and the data are noisy. The MIPAS FR and RR periods were considered together in the balloon validation due to limited reference profiles and comparisons in the FR period. The results shown here for MLS are all for v5. For MkIV, the 1 April 2003 Kiruna flight was separated from the other Kiruna flights because no polar vortex air was sampled, resulting in significantly different VMRs above 25 km. For GLORIA and MIPAS-B, all flights included some vortex air so they were not separated.

Summary plots were also created for easily comparing the performances of each instrument relative to the balloon datasets. For each region, the median relative differences at 13 km, 18 km, 23 km, and 28 km are shown as a grid plot, with each panel corresponding to the comparisons with one balloon instrument. 13 km was chosen as the fourth level here because the mean relative biases are very large at 33 km, even more so than with the intercomparisons due to the smaller number of coincidences available. Positive values correspond to a high bias in the satellite instrument and vice versa. As with the intercomparison summary plots, the absolute differences are written on each box in ppbv as well as the relative differences. The colour gradient

https://doi.org/10.5194/egusphere-2026-4651
Preprint. Discussion started: 18 August 2026

is limited to −50 to 50%, and boxes with relative differences of greater magnitude do not have a colored border. This is because in most cases, the relative differences are that large simply due to smaller VMRs, and they are therefore not indicative of any major issues with the satellite dataset.

4.2 Validation results

The mean profile comparisons with GLORIA-B are shown in Figure 14. In the midlatitudes, ACE-FTS and SMR have a very similar level of agreement with GLORIA-B above 18 km; both have a low bias of about 5% between 18 and 21 km, then a high bias of 5-10% from 21-27 km. The biases oscillate similarly above 27 km, to a maximum high bias of 20% for ACE-FTS and about 30% for SMR at 31 km and then reduces to a negative bias of 45% for ACE-FTS and nearly −55% for SMR at 35 km. The deviation in the MLS v5 profile near 25 km is apparent and results in a low bias of up to 30% at altitudes below 26 km. Above 27 km, the MLS v5 bias oscillates similarly to ACE-FTS and SMR, to a maximum value of 35% at 31 km and a minimum value of −20% at 35 km.

The agreement with the mean GLORIA-B profile is less consistent between satellite instruments in the Arctic. The ACE-FTS bias is within ±15% up to 27 km, above which the bias decreases to −20% at 29 km, increases to zero at 31 km, then decreases to −90% at 36 km. As in the midlatitudes, MLS v5 has a low bias of about 25% up to 25 km, above which the bias crosses zero at 27 km and increases to nearly 60% at 32 km, then decreases to -55% at 36 km. The SMR bias is negative from 15-21 km, then positive from 21-27 km, and always within ±20%. Below about 18 km, however, the low bias is quite significant compared to the estimated balloon uncertainty. These validation results are fairly consistent with those of the intercomparisons: the MLS v5 deviation reduces its reliability, but ACE-FTS and SMR perform well.

The comparisons with MIPAS-B are shown in Figure 15. In the tropics, HIRDLS, MIPAS (both datasets), and SMR all have positive biases within 20% from 18-31 km. Of the four datasets, SMR has the smallest bias; in fact it is less than ±10% over the entire altitude range (14-37 km). The MLS v5 bias is also within ±10% except at 34 km where it is slightly more negative than −10%. However, the profile shape still differs from that of the mean balloon profile due to the deviation. The HIRDLS profile is oddly shaped below 20 km, where the N_2O VMR decreases at lower altitudes, resulting in a deviation of −10% at 17 km, the lowest available altitude. This is not expected behaviour for N_2O and is likely due to an issue in the dataset. The MIPAS-B mean profile exhibits some strange behaviour above 33 km; there is a jump from about 135 ppbv to 145 ppbv at 34 km as a result of averaging balloon profiles together. This results in MIPAS, MLS v5, and SMR all having low biases of up to about 10% between 33 and 36 km, though the satellite VMRs are within the balloon's uncertainty estimate.

In the midlatitudes, ACE-FTS and SMR agree best with MIPAS-B; both are within ±10% from 14-30 km. The satellite datasets mostly have positive biases in the lower stratosphere below 22 km, with the exception of SMR which has a small negative bias of about 5% below 15 km. They are all within the MIPAS-B measurement uncertainty range at these altitudes, except for the MIPAS datasets below 14 km where the uncertainties in the satellite measurements still make this difference insignificant. There is a deviation in the mean balloon profile between 13 and 14 km, which is because the Timmins profiles from 2014 do not extend below 14 km and are therefore excluded from the mean. MIPAS did not coincide with these profiles, though, so this does not affect the mean of the relative differences in the rightmost panel. The MIPAS datasets both have positive mean biases all the way from 9-33 km, ranging from 2-25%. The deviation in the MLS v5 profile is again apparent and results in a negative bias of over 30% at 24 km. Aside from this, the satellite profiles are mostly consistent with the MIPAS-B profile from 14-30 km.

The Arctic comparisons for ACE-FTS, SMR, and the two MIPAS datasets with MIPAS-B are also very good. Based on the profile comparisons on the left side, they are consistent with the mean balloon profile up to about 29 km except at about 22-23 km where the SMR and MIPAS-IMK have sharper changes in slope and therefore small negative deviations of about 10% and 5%, respectively. Above 25 km, the mean relative biases are quite high, over 50%, for all instruments. At these altitudes with small VMRs, one comparison can strongly skew the mean relative bias. MLS v5 has an even larger high bias from 21-33 km of over 100%. It is the only satellite dataset that does not fully capture the decrease in N_2O caused by descent within the polar vortex. Below 21 km, however, the agreement between MLS v5 and MIPAS-B is good aside from a positive bias of about 30% between 16 and 18 km.

The profile comparisons with MkIV are shown in Figure 16. In the midlatitudes, ACE-FTS, MIPAS (both datasets), and SMR are consistent with the mean balloon profile from 9-32 km. However, SMR does have a low bias of just under 10% below 19 km, while ACE-FTS and MIPAS are within $\pm 5\%$ up to 19 km. The deviation in the MLS v5 profile again results in a negative bias, of up to 20% here, between 20 and 25 km. All of the satellite instruments have positive biases betwen 31 and 37 km, the largest being for HIRDLS (over 75% at 33 km). They all have a negative bias at the highest altitudes (39-40 km), but they cross the zero bias line at different altitudes. HIRDLS has a high bias from 25-31 km as well, of up to 30%, but its negative bias from 18-24 km is within 10%. Based on these comparisons, ACE-FTS and MIPAS are very reliable datasets, SMR is reliable above 19 km, and MLS v5 and HIRDLS should be used with caution.

The MkIV Arctic comparisons are based on only three flights: one in 2002, one in 2003, and one in 2007. No polar vortex air was sampled during the 2003 flight, so it was separated from the other two for this analysis. The negative VMR at 25 km for the 2007 flight was deemed an outlier and removed. The results including the two flights within the polar vortex are shown in the middle row of Figure 16. The satellite profiles in the left panel are very similar to each other; MIPAS-ESA, MIPAS-IMK, and SMR all have negative biases of up to about 40 ppbv (around 50% at 20 km) from 9-21 km. The MIPAS-ESA bias is slightly larger (i.e., more negative) than the other two, by about 20 ppbv between 19 and 21 km. The mean relative biases in the right panels are within -25% below 20 km. Both MIPAS profiles and the SMR profile are all consistent with the balloon profile everywhere except 16 km and 20 km. From 25-34 km, all six datasets have slightly positive biases (according to the left panel), but are still consistent with the balloon profile. The mean relative biases in the right panel are very large (up to over 100%) and noisy due to the small VMRs at these altitudes. The comparisons with the 2003 flight are shown in the bottom panel of Figure 16. The satellite profiles are consistent with the balloon profile everywhere except at 28 km, where the MkIV profile has a slight positive deviation, likely due to the comparison being based on a single MkIV profile. MIPAS-IMK has a positive bias of up to 17% from 17-26 km, but it is not statistically significant. All three datasets (MIPAS-ESA, MIPAS-IMK, and SMR) have a negative bias between 12 and 16 km, SMR having the largest by about 20 ppbv at 12 km, but this is also not statistically significant.

https://doi.org/10.5194/egusphere-2026-4651
Preprint. Discussion started: 18 August 2026

The validation is summarized in Figures 17, 18, and 19 for the tropics, midlatitudes, and Arctic, respectively. MIPAS-B is the only balloon instrument with any tropical flights. The agreement is very good; all relative differences are within 20% and 13 of 17 boxes have relative differences within 10%. The biases in the satellite instruments are mostly positive (15 of 17 boxes), which as previously noted could instead indicate a negative bias in MIPAS-B, especially at 23 km and 28 km where all the satellite biases are positive except for MLS v5 at 23 km, where it is known to be unreliable.

Figure 18 shows that overall, the satellite-balloon agreement is very good; only 3 of 48 boxes have relative differences with a magnitude greater than 20%, and 33 boxes have relative differences that are within 10%. There are some notable patterns, however. For example, all the satellite biases are positive at 18 km when compared with MIPAS-B, all are negative at 18 km and 28 km when compared with GLORIA-B, all are negative at 23 km when compared with MkIV, and all are positive at 28 km when compared with MkIV. Systematic differences such as these suggest that the bias could be in the balloon instruments rather than the satellite instruments. However, it is unclear at 18 km whether the bias relative to GLORIA-B (negative) or the bias relative to MIPAS-B (positive) is real. Regardless, the agreement is good enough that the satellite datasets can be considered usable at this altitude. For MkIV, the differences are related to the upward concavity in the profile starting near 30 km in the midlatitudes. The GLORIA-B profiles do not have this concavity, but as they are mean profiles and not from individual measurements, the situations are not entirely comparable.

The summary for the Arctic in Figure 19, which only includes flights within the vortex (i.e., all but the 2003 MkIV flight), shows that there are large relative differences at 28 km, but this is expected given the low VMRs caused by air descent in the polar vortex. Aside from this, there is generally good agreement between the satellite and balloon datasets. Of the 35 boxes with coloured borders, only 5 have relative differences with magnitudes greater than 20%, and 18 have relative differences within ±10%. All of the biases relative to MIPAS-B are positive, further indicating that MIPAS-B itself may have a negative bias. That said, there are no previous studies that indicate this could be the case. The differences relative to GLORIA-B are mostly negative, particularly at lower altitudes. There is also a pattern in the MkIV comparisons: The instrument biases are negative at lower altitudes (13 km and 18 km) and then positive at higher altitudes. This aligns with Figure 16, which suggests that in the Arctic vortex, the satellite instrument profiles are slightly less steep than the mean MkIV profile. However, the difference is not statistically significant except at 20 km where the MkIV profile has the deviation, likely due to the comparison being based on a single MkIV profile in this altitude range.

5 Summary

In support of the LOLIPOP project, evaluations of N_2O measurements from six different satellite datasets (ACE-FTS, HIRDLS, MIPAS-ESA, MIPAS-IMK, MLS, and SMR) were presented in two parts: intercomparisons between the instruments being evaluated and validation through comparisons with a series of balloon-borne reference instruments (GLORIA-B, MIPAS-B, and MkIV). Several coincidence-finding methods and criteria were tested, and the criteria were eventually chosen in order to maximize the number of coincidences available without significantly detracting from the agreement between datasets. For the intercomparisons, median profile-to-profile comparisons for different regions and times of year were presented as well

https://doi.org/10.5194/egusphere-2026-4651
Preprint. Discussion started: 18 August 2026

as PDFs at four selected altitudes in the upper troposphere and lower-to-middle stratosphere. The results from SMR were highlighted because it had the greatest temporal overlap with the other instruments and was found to have generally high-quality measurements. The intercomparisons were also summarized in grid plots for easier identification of patterns in the biases. The validation comparisons using independent reference data were separated by balloon instrument and by latitude band (tropics, northern midlatitudes, and Arctic) and included mean profile-to-profile comparisons as well as summary grid plots.

Overall, the intercomparisons indicated that the satellite datasets are generally very reliable, with few exceptions. In particular, ACE-FTS, MIPAS (both datasets), and SMR agreed well with each other in most regions. The ACE-FTS and MIPAS biases relative to SMR were typically within ±5% and at worst still within ±10%. The largest biases were generally found at the upper and lower ends of the profiles, the former due to low VMRs and the latter due to difficulty in measuring in the upper troposphere. HIRDLS had variable performance; the profiles agreed better in some regions than others, where sometimes the HIRDLS profile had much more structure (i.e., had more changes in vertical gradient) than the others. It is therefore recommended that the comparisons for the region and time period of interest be consulted before making use of this dataset. The HIRDLS results also support the instrument team's recommendation to only use zonal mean data rather than the individual profiles. Outside of the polar vortex, MLS v5 N_2O profiles have a deviation centred near 24 km (around the 32 hPa level) that results in a negative bias from about 20-25 km as large as 30%. This is a significant issue in the dataset that has been addressed, and users are encouraged to use the improved MLS version 6 N_2O retrievals. These results were corroborated through validation with balloon instruments. On average, the satellite profiles agreed with the balloon profiles within ±10% in most cases and if not, within ±20% unless the VMR was very small, as it is above 22 km in the Arctic due to air descent within the polar vortex. Differences between the individual satellites and the balloon instruments were generally larger than those between satellite instruments, possibly due to the smaller number of coincidences available. All in all, only HIRDLS and MLS v5 N_2O measurements had significant issues identified. Otherwise, the currently available satellite limb-viewing N_2O datasets were found to be of very high quality. Together, ACE-FTS, MIPAS, SMR, and possibly MLS v6 constitute an excellent 24-year record of N_2O measurements. With some adjustments to account for biases, they could be merged into a continuous time series, in the framework of the ESA Climate Change Initiative, for future trend analysis and examination of changes in stratospheric circulation.

Data availability. ACE-FTS data can be obtained via the ACE-FTS website (registration required; ACE-FTS, 2024). HIRDLS data are available on the Goddard Earth Sciences Data and Information Services Centre (GES DISC; Gille and Gray, 2013b). The MIPAS-ESA dataset is available on the Earth Online repository (registration required; European Space Agency, 2021). The MIPAS-IMK data are available from the KITopen repository (Glatthor et al., 2024b). The MLS v5 and v6 data are available on GES DISC (Lambert et al., 2020, 2026). The SMR data are available on the Odin-SMR website (Odin-SMR, 2023). GLORIA-B measurements are available on the KITopen repository (Wetzel and Johansson, 2025a, b). MIPAS-B data are available upon request from one of the co-authors (gerald.wetzel@kit.edu). The MkIV data are available on the JPL website (Jet Propulsion Laboratory, 2024). The JPL Derived Meteorological Products are available upon request from one of the co-authors (luis.f.millan@jpl.nasa.gov).

https://doi.org/10.5194/egusphere-2026-4651
Preprint. Discussion started: 18 August 2026

Author contributions. This study was conceptualized by KAW and GPS. LNS performed the analysis, designed the figures, and wrote the manuscript, with input from KAW, GPS, and PR. GPS, along with NG, provided their expertise on the MIPAS-IMK dataset. PR provided their expertise on the MIPAS-ESA dataset. LFM produced the Derived Meteorological Products for each of the satellite and balloon datasets. MG created the MIPAS-ESA harmonized data files. CDB and PES provided their expertise on ACE-FTS; JG provided their expertise on HIRDLS; AL provided their expertise on MLS; GW and A Kleinert provided their expertise on the GLORIA-B and MIPAS-B datasets; A Kleinböhl and GCT provided their expertise on the MkIV dataset. All authors provided valuable comments on the manuscript.

Competing interests. At least one co-author is an editor of Atmospheric Measurement Techniques.

Acknowledgements. This work has been performed in the framework of the ESA LOLIPOP project. The Atmospheric Chemistry Experiment (ACE) is a Canadian-led mission mainly supported by the Canadian Space Agency. We thank the European Space Agency (ESA) for its support in producing, improving, and making publicly available the MIPAS Level-2 dataset. We thank Rashid Khosravi for his work on the HIRDLS v07 N_2O dataset. Work at the Jet Propulsion Laboratory, California Institute of Technology, is performed under contract with the National Aeronautics and Space Administration (80NM0018D0004). A Kleinböhl and GCT acknowledge support from NASA's Upper Atmosphere Composition Observations Program (80NM0018F0583). We thank the Centre National d'Études Spatiales (CNES) and the Swedish Space Corporation (SSC) for the excellent balloon operations of the MIPAS-B and GLORIA-B instruments.

https://doi.org/10.5194/egusphere-2026-4651
Preprint. Discussion started: 18 August 2026

References

ACE-FTS: Level 2 Data, Version 5.2, ACE-FTS [data set], https://databace.scisat.ca/level2/, accessed 12 April 2024, 2024.

Bernath, P. F., McElroy, C. T., Abrams, M. C., Boone, C. D., Butler, M., Camy-Peyret, C., Carleer, M., Clerbaux, C., Coheur, P.-F., Colin, R., DeCola, P., DeMazière, M., Drummond, J. R., Dufour, D., Evans, W. F. J., Fast, H., Fussen, D., Gilbert, K., Jennings, D. E., Llewellyn, E. J., Lowe, R. P., Mahieu, E., McConnell, J. C., McHugh, M., McLeod, S. D., Michaud, R., Midwinter, C., Nassar, R., Nichitiu, F., Nowlan, C., Rinsland, C. P., Rochon, Y. J., Rowlands, N., Semeniuk, K., Simon, P., Skelton, R., Sloan, J. J., Soucy, M.-A., Strong, K., Tremblay, P., Turnbull, D., Walker, K. A., Walkty, I., Wardle, D. A., Wehrle, V., Zander, R., and Zou, J.: Atmospheric Chemistry Experiment (ACE): Mission overview, Geophysical Research Letters, 32, L15S01, https://doi.org/10.1029/2005GL022386, 2005.

Boone, C., Bernath, P., and Lecours, M.: Version 5 retrievals for ACE-FTS and ACE-imagers, Journal of Quantitative Spectroscopy and Radiative Transfer, 310, 108 749, https://doi.org/10.1016/j.jqsrt.2023.108749, 2023.

Dinelli, B. M., Raspollini, P., Gai, M., Sgheri, L., Ridolfi, M., Ceccherini, S., Barbara, F., Zoppetti, N., Castelli, E., Papandrea, E., Pettinari, P., Dehn, A., Dudhia, A., Kiefer, M., Piro, A., Flaud, J.-M., López-Puertas, M., Moore, D., Remedios, J., and Bianchini, M.: The ESA MIPAS/Envisat level2-v8 dataset: 10 years of measurements retrieved with ORM v8.22, Atmospheric Measurement Techniques, 14, 7975–7998, https://doi.org/10.5194/amt-14-7975-2021, 2021.

Douglass, A. R., Prather, M. J., Hall, T. M., Strahan, S. E., Rasch, P. J., Sparling, L. C., Coy, L., and Rodriguez, J. M.: Choosing meteorological input for the global modeling initiative assessment of high-speed aircraft, Journal of Geophysical Research: Atmospheres, 104, 27 545–27 564, https://doi.org/10.1029/1999JD900827, 1999.

Drummond, J. R., Houghton, J. T., Peskett, G. D., Rodgers, C. D., Wale, M. J., Whitney, J., Williamson, E. J., Massey, H. S. W., Beynon, W. J. G., Houghton, J. T., and Thomas, L.: The stratospheric and mesospheric sounder on Nimbus 7, Philosophical Transactions of the Royal Society of London. Series A, Mathematical and Physical Sciences, 296, 219–241, https://doi.org/10.1098/rsta.1980.0166, 1980.

Dubé, K., Tegtmeier, S., Bourassa, A., Zawada, D., Degenstein, D., Sheese, P. E., Walker, K. A., and Randel, W.: N_2O as a regression proxy for dynamical variability in stratospheric trace gas trends, Atmospheric Chemistry and Physics, 23, 13 283–13 300, https://doi.org/10.5194/acp-23-13283-2023, 2023.

Dubé, K., Tegtmeier, S., Ploeger, F., and Walker, K. A.: Hemispheric asymmetry in recent stratospheric age of air changes, Atmospheric Chemistry and Physics, 25, 1433–1447, https://doi.org/10.5194/acp-25-1433-2025, 2025.

Ejiri, M. K., Terao, Y., Sugita, T., Nakajima, H., Yokota, T., Toon, G. C., Sen, B., Wetzel, G., Oelhaf, H., Urban, J., Murtagh, D., Irie, H., Saitoh, N., Tanaka, T., Kanzawa, H., Shiotani, M., Aoki, S., Hashida, G., Machida, T., Nakazawa, T., Kobayashi, H., and Sasano, Y.: Validation of the Improved Limb Atmospheric Spectrometer-II (ILAS-II) Version 1.4 nitrous oxide and methane profiles, Journal of Geophysical Research: Atmospheres, 111, D22S90, https://doi.org/10.1029/2005JD006449, 2006.

European Space Agency: Envisat MIPAS L2 - Temperature, pressure and atmospheric constituents profiles. Version 8.22 [data set], https://doi.org/10.5270/EN1-c8hgqx4, accessed 15 July 2026, 2021.

Fischer, H., Birk, M., Blom, C., Carli, B., Carlotti, M., von Clarmann, T., Delbouille, L., Dudhia, A., Ehhalt, D., Endemann, M., Flaud, J. M., Gessner, R., Kleinert, A., Koopman, R., Langen, J., López-Puertas, M., Mosner, P., Nett, H., Oelhaf, H., Perron, G., Remedios, J., Ridolfi, M., Stiller, G., and Zander, R.: MIPAS: an instrument for atmospheric and climate research, Atmospheric Chemistry and Physics, 8, 2151–2188, https://doi.org/10.5194/acp-8-2151-2008, 2008.

Forster, P., Storelvmo, T., Armour, K., Collins, W., Dufresne, J.-L., Frame, D., Lunt, D., Mauritsen, T., Palmer, M., Watanabe, M., Wild, M., and Zhang, H.: The Earth's Energy Budget, Climate Feedbacks, and Climate Sensitivity, in: Climate Change 2021: The Physical Science

Basis. Contribution of Working Group I to the Sixth Assessment Report of the Intergovernmental Panel on Climate Change, edited by Masson-Delmotte, V., Zhai, P., Pirani, A., Connors, S., C. Péan, S. B., Caud, N., Chen, Y., Goldfarb, L., Gomis, M., Huang, M., Leitzell, K., Lonnoy, E., Matthews, J., Maycock, T., Waterfield, T., Yelekçi, O., Yu, R., and Zhou, B., pp. 923–1054, Cambridge University Press, Cambridge, United Kingdom and New York, NY, USA, https://doi.org/10.1017/9781009157896.009, 2021.

Friedl-Vallon, F., Maucher, G., Seefeldner, M., Trieschmann, O., Kleinert, A., Lengel, A., Keim, C., Oelhaf, H., and Fischer, H.: Design and characterization of the balloon-borne Michelson Interferometer for Passive Atmospheric Sounding (MIPAS-B2), Applied Optics, 43, 3335–3355, https://doi.org/10.1364/AO.43.003335, 2004.

Friedl-Vallon, F., Gulde, T., Hase, F., Kleinert, A., Kulessa, T., Maucher, G., Neubert, T., Olschewski, F., Piesch, C., Preusse, P., Rongen, H., Sartorius, C., Schneider, H., Schönfeld, A., Tan, V., Bayer, N., Blank, J., Dapp, R., Ebersoldt, A., Fischer, H., Graf, F., Guggenmoser, T., Höpfner, M., Kaufmann, M., Kretschmer, E., Latzko, T., Nordmeyer, H., Oelhaf, H., Orphal, J., Riese, M., Schardt, G., Schillings, J., Sha, M. K., Suminska-Ebersoldt, O., and Ungermann, J.: Instrument concept of the imaging Fourier transform spectrometer GLORIA, Atmospheric Measurement Techniques, 7, 3565–3577, https://doi.org/10.5194/amt-7-3565-2014, 2014.

Funke, B., García-Comas, M., López-Puertas, M., Glatthor, N., Stiller, G. P., von Clarmann, T., Semeniuk, K., and McConnell, J. C.: Enhancement of N_2O during the October–November 2003 solar proton events, Atmospheric Chemistry and Physics, 8, 3805–3815, https://doi.org/10.5194/acp-8-3805-2008, 2008.

Garny, H., Ploeger, F., Abalos, M., Bönisch, H., Castillo, A., von Clarmann, T., Diallo, M., Engel, A., Laube, J., Linz, M., Neu, J., Podglajen, A., Ray, E., Rivoire, L., Saunders, L., Stiller, G., Voet, F., Wagenhäuser, T., and Walker, K.: Age of stratospheric air: Progress on processes, observations and long-term trends, Reviews of Geophysics, 62, e2023RG000 832, https://doi.org/10.1029/2023RG000832, 2024.

Gelaro, R., McCarty, W., Suárez, M. J., Todling, R., Molod, A., Takacs, L., Randles, C. A., Darmenov, A., Bosilovich, M. G., Reichle, R., Wargan, K., Coy, L., Cullather, R., Draper, C., Akella, S., Buchard, V., Conaty, A., da Silva, A. M., Gu, W., Kim, G.-K., Koster, R., Lucchesi, R., Merkova, D., Nielsen, J. E., Partyka, G., Pawson, S., Putman, W., Rienecker, M., Schubert, S. D., Sienkiewicz, M., and Zhao, B.: The Modern-Era Retrospective Analysis for Research and Applications, Version 2 (MERRA-2), Journal of Climate, 30, 5419–5454, https://doi.org/10.1175/JCLI-D-16-0758.1, 2017.

Gille, J. and Gray, L.: High Resolution Dynamics Limb Sounder Earth Observing System (EOS) Data Description and Quality Version 7 (V7) (HIRDLS Version 7.00.00), National Aeronautics and Space Administration (NASA), available online: https://docserver.gesdisc.eosdis.nasa.gov/repository/Mission/HIRDLS/3.3_Product_Documentation/3.3.5_Product_Quality/HIRDLS-DQD_V7.pdf, accessed on 26 November 2025, 2013a.

Gille, J. and Gray, L. J.: HIRDLS/Aura Level 2 Geophysical Parameters (on a pressure grid) V007, https://doi.org/10.5067/Aura/HIRDLS/DATA201, accessed 2 April 2024, 2013b.

Gille, J., Barnett, J., Arter, P., Barker, M., Bernath, P., Boone, C., Cavanaugh, C., Chow, J., Coffey, M., Craft, J., Craig, C., Dials, M., Dean, V., Eden, T., Edwards, D. P., Francis, G., Halvorson, C., Harvey, L., Hepplewhite, C., Khosravi, R., Kinnison, D., Krinsky, C., Lambert, A., Lee, H., Lyjak, L., Loh, J., Mankin, W., Massie, S., McInerney, J., Moorhouse, J., Nardi, B., Packman, D., Randall, C., Reburn, J., Rudolf, W., Schwartz, M., Serafin, J., Stone, K., Torpy, B., Walker, K., Waterfall, A., Watkins, R., Whitney, J., Woodard, D., and Young, G.: High Resolution Dynamics Limb Sounder: Experiment overview, recovery, and validation of initial temperature data, Journal of Geophysical Research: Atmospheres, 113, D16S43, https://doi.org/10.1029/2007JD008824, 2008.

Glatthor, N., von Clarmann, T., Funke, B., García-Comas, M., Grabowski, U., Höpfner, M., Kellmann, S., Kiefer, M., Laeng, A., Linden, A., López-Puertas, M., and Stiller, G. P.: IMK–IAA MIPAS retrieval version 8: CH_4 and N_2O, Atmospheric Measurement Techniques, 17, 2849–2871, https://doi.org/10.5194/amt-17-2849-2024, 2024a.

https://doi.org/10.5194/egusphere-2026-4651
Preprint. Discussion started: 18 August 2026

Glatthor, N., von Clarmann, T., Funke, B., García-Comas, M., Grabowski, U., Höpfner, M., Kellmann, S., Kiefer, M., Laeng, A., Linden, A., López-Puertas, M., and Stiller, G. P.: IMK–IAA MIPAS retrieval version 8: N_2O, the data set, https://doi.org/10.35097/1949, accessed 25 June 2026, 2024b.

Gunson, M. R., Abbas, M. M., Abrams, M. C., Allen, M., Brown, L. R., Brown, T. L., Chang, A. Y., Goldman, A., Irion, F. W., Lowes, L. L., Mahieu, E., Manney, G. L., Michelsen, H. A., Newchurch, M. J., Rinsland, C. P., Salawitch, R. J., Stiller, G. P., Toon, G. C., Yung, Y. L., and Zander, R.: The Atmospheric Trace Molecule Spectroscopy (ATMOS) Experiment: Deployment on the ATLAS space shuttle missions, Geophysical Research Letters, 23, 2333–2336, https://doi.org/10.1029/96GL01569, 1996.

Jet Propulsion Laboratory: MkIV Balloon Profiles [data set], https://mark4sun.jpl.nasa.gov/m4data.html, accessed 15 July 2025, 2024.

Kanzawa, H., Sugita, T., Nakajima, H., Bodeker, G. E., Oelhaf, H., Stowasser, M., Wetzel, G., Engel, A., Schmidt, U., Levin, I., Toon, G. C., Sen, B., Blavier, J.-F., Aoki, S., Nakazawa, T., Jucks, K. W., Johnson, D. G., Traub, W. A., Camy-Peyret, C., Payan, S., Jeseck, P., Murata, I., Fukunishi, H., von König, M., Bremer, H., Küllmann, H., Park, J. H., Pan, L. L., Yokota, T., Suzuki, M., Shiotani, M., and Sasano, Y.: Validation and data characteristics of nitrous oxide and methane profiles observed by the Improved Limb Atmospheric Spectrometer (ILAS) and processed with the Version 5.20 algorithm, Journal of Geophysical Research: Atmospheres, 108, 8003, https://doi.org/10.1029/2002JD002458, 2003.

Khosravi, R., Lambert, A., Lee, H., Gille, J., Barnett, J., Francis, G., Edwards, D., Halvorson, C., Massie, S., Craig, C., Krinsky, C., McInerney, J., Stone, K., Eden, T., Nardi, B., Hepplewhite, C., Mankin, W., and Coffey, M.: Overview and characterization of retrievals of temperature, pressure, and atmospheric constituents from the High Resolution Dynamics Limb Sounder (HIRDLS) measurements, Journal of Geophysical Research: Atmospheres, 114, D20304, https://doi.org/10.1029/2009JD011937, 2009.

Kolonjari, F., Plummer, D. A., Walker, K. A., Boone, C. D., Elkins, J. W., Hegglin, M. I., Manney, G. L., Moore, F. L., Pendlebury, D., Ray, E. A., Rosenlof, K. H., and Stiller, G. P.: Assessing stratospheric transport in the CMAM30 simulations using ACE-FTS measurements, Atmospheric Chemistry and Physics, 18, 6801–6828, https://doi.org/10.5194/acp-18-6801-2018, 2018.

Krysztofiak, G., Catoire, V., Dudok de Wit, T., Kinnison, D. E., Ravishankara, A. R., Brocchi, V., Atlas, E., Bozem, H., Commane, R., D'Amato, F., Daube, B., Diskin, G. S., Engel, A., Friedl-Vallon, F., Hintsa, E., Hurst, D. F., Hoor, P., Jegou, F., Jucks, K. W., Kleinböhl, A., Küllmann, H., Kort, E. A., McKain, K., Moore, F. L., Obersteiner, F., Ramos, Y. G., Schuck, T., Toon, G. C., Viciani, S., Wetzel, G., Williams, J., and Wofsy, S. C.: N_2O Temporal Variability from the Middle Troposphere to the Middle Stratosphere Based on Airborne and Balloon-Borne Observations during the Period 1987–2018, Atmosphere, 14, 585, https://doi.org/10.3390/atmos14030585, 2023.

Lambert, A., Read, W. G., Livesey, N. J., Santee, M. L., Manney, G. L., Froidevaux, L., Wu, D. L., Schwartz, M. J., Pumphrey, H. C., Jimenez, C., Nedoluha, G. E., Cofield, R. E., Cuddy, D. T., Daffer, W. H., Drouin, B. J., Fuller, R. A., Jarnot, R. F., Knosp, B. W., Pickett, H. M., Perun, V. S., Snyder, W. V., Stek, P. C., Thurstans, R. P., Wagner, P. A., Waters, J. W., Jucks, K. W., Toon, G. C., Stachnik, R. A., Bernath, P. F., Boone, C. D., Walker, K. A., Urban, J., Murtagh, D., Elkins, J. W., and Atlas, E.: Validation of the Aura Microwave Limb Sounder middle atmosphere water vapor and nitrous oxide measurements, Journal of Geophysical Research: Atmospheres, 112, D24S36, https://doi.org/10.1029/2007JD008724, 2007.

Lambert, A., Livesey, N., and Read, W.: MLS/Aura Level 2 Nitrous Oxide (N2O) Mixing Ratio V005, https://doi.org/10.5067/Aura/MLS/DATA2515, accessed 2 April 2024, 2020.

Lambert, A., Livesey, N., and Read, W.: MLS/Aura Level 2 Nitrous Oxide (N2O) Mixing Ratio V006, https://doi.org/10.5067/Aura/MLS/DATA2615, accessed 28 May 2026, 2026.

Linz, M., Plumb, R. A., Gerber, E. P., Haenel, F. J., Stiller, G., Kinnison, D. E., Ming, A., and Neu, J. L.: The strength of the meridional overturning circulation of the stratosphere, Nature Geoscience, 10, 663–667, https://doi.org/10.1038/ngeo3013, 2017.

Livesey, N. J., Read, W. G., Wagner, P. A., Froidevaux, L., Santee, M. L., Schwartz, M. J., Lambert, A., Valle, L. F. M., Pumphrey, H. C., Manney, G. L., Fuller, R. A., Jarnot, R. F., Knosp, B. W., and Lay, R. R.: Version 5.0x Level 2 and 3 data quality and description document (Version 5.0-1.1a), Tech. Rep. D-105336 Rev. B, Jet Propulsion Laboratory, available online: https://mls.jpl.nasa.gov/data/v5-0_data_quality_document.pdf, accessed on 12 September 2024, 2022.

Livesey, N. J., Read, W. G., Santee, M. L., Froidevaux, L., , Schwartz, M. J., Lambert, A., Valle, L. F. M., Warner, F., Pumphrey, H. C., Manney, G. L., Fuller, R. A., Jarnot, R. F., Knosp, B. W., and Vuu, C.: Version 6.0x Level-2 and Level-3 data quality and description document, https://doi.org/10.5067/AURA/MLS/DOC/v6_dataqualitydocument, accessed on 8 July 2026, 2026.

Manney, G. L., Daffer, W. H., Zawodny, J. M., Bernath, P. F., Hoppel, K. W., Walker, K. A., Knosp, B. W., Boone, C., Remsberg, E. E., Santee, M. L., Harvey, V. L., Pawson, S., Jackson, D. R., Deaver, L., McElroy, C. T., McLinden, C. A., Drummond, J. R., Pumphrey, H. C., Lambert, A., Schwartz, M. J., Froidevaux, L., McLeod, S., Takacs, L. L., Suarez, M. J., Trepte, C. R., Cuddy, D. C., Livesey, N. J., Harwood, R. S., and Waters, J. W.: Solar occultation satellite data and derived meteorological products: Sampling issues and comparisons with Aura Microwave Limb Sounder, Journal of Geophysical Research: Atmospheres, 112, D24S50, https://doi.org/10.1029/2007JD008709, 2007.

Manney, G. L., Hegglin, M. I., Daffer, W. H., Santee, M. L., Ray, E. A., Pawson, S., Schwartz, M. J., Boone, C. D., Froidevaux, L., Livesey, N. J., Read, W. G., and Walker, K. A.: Jet characterization in the upper troposphere/lower stratosphere (UTLS): applications to climatology and transport studies, Atmospheric Chemistry and Physics, 11, 6115–6137, https://doi.org/10.5194/acp-11-6115-2011, 2011.

Manney, G. L., Millán, L. F., Santee, M. L., Wargan, K., Lambert, A., Neu, J. L., Werner, F., Lawrence, Z. D., Schwartz, M. J., Livesey, N. J., and Read, W. G.: Signatures of Anomalous Transport in the 2019/2020 Arctic Stratospheric Polar Vortex, Journal of Geophysical Research: Atmospheres, 127, e2022JD037407, https://doi.org/10.1029/2022JD037407, 2022.

Millán, L. F., Manney, G. L., Boenisch, H., Hegglin, M. I., Hoor, P., Kunkel, D., Leblanc, T., Petropavlovskikh, I., Walker, K., Wargan, K., and Zahn, A.: Multi-parameter dynamical diagnostics for upper tropospheric and lower stratospheric studies, Atmospheric Measurement Techniques, 16, 2957–2988, https://doi.org/10.5194/amt-16-2957-2023, 2023.

Minganti, D., Chabrillat, S., Errera, Q., Prignon, M., Kinnison, D. E., Garcia, R. R., Abalos, M., Alsing, J., Schneider, M., Smale, D., Jones, N., and Mahieu, E.: Evaluation of the N_2O Rate of Change to Understand the Stratospheric Brewer-Dobson Circulation in a Chemistry-Climate Model, Journal of Geophysical Research: Atmospheres, 127, e2021JD036390, https://doi.org/10.1029/2021JD036390, 2022.

Murtagh, D., Frisk, U., Merino, F., Ridal, M., Jonsson, A., Stegman, J., Witt, G., Eriksson, P., Jiménez, C., Megie, G., Noë, J. d. l., Ricaud, P., Baron, P., Pardo, J. R., Hauchcorne, A., Llewellyn, E. J., Degenstein, D. A., Gattinger, R. L., Lloyd, N. D., Evans, W. F., McDade, I. C., Haley, C. S., Sioris, C., Savigny, C. v., Solheim, B. H., McConnell, J. C., Strong, K., Richardson, E. H., Leppelmeier, G. W., Kyrölä, E., Auvinen, H., and Oikarinen, L.: An overview of the Odin atmospheric mission, Canadian Journal of Physics, 80, 309–319, https://doi.org/10.1139/p01-157, 2002.

NOAA: Trends in CO_2, CH_4, N_2O, SF_6, https://gml.noaa.gov/ccgg/trends/, accessed on 7 May 2026, 2026.

Odin-SMR: Odin/SMR Data Access, https://odin-smr.org/data_access, accessed 15 July 2025, 2023.

Prather, M. J., Hsu, J., DeLuca, N. M., Jackman, C. H., Oman, L. D., Douglass, A. R., Fleming, E. L., Strahan, S. E., Steenrod, S. D., Søvde, O. A., Isaksen, I. S. A., Froidevaux, L., and Funke, B.: Measuring and modeling the lifetime of nitrous oxide including its variability, Journal of Geophysical Research: Atmospheres, 120, 5693–5705, https://doi.org/10.1002/2015JD023267, 2015.

Raspollini, P., Piro, A., Hubert, D., Keppens, A., Lambert, J.-C., Wetzel, G., Moore, D., Ceccherini, S., Gai, M., Barbara, F., and Zoppetti, N.: ESA Level 2 version 8.22 products - Product Quality Readme File, Tech. Rep. ESA-EOPG-EBA-TN-5, European Space Agency, available online: https://earth.esa.int/eogateway/documents/20142/37627/README_V8_issue_1.1_20210916.pdf/0983f031-c54f-f089-fe61-6f24ccf4d4f3, accessed on 16 June 2026, 2021.

Raspollini, P., Arnone, E., Barbara, F., Bianchini, M., Carli, B., Ceccherini, S., Chipperfield, M. P., Dehn, A., Della Fera, S., Dinelli, B. M., Dudhia, A., Flaud, J.-M., Gai, M., Kiefer, M., López-Puertas, M., Moore, D. P., Piro, A., Remedios, J. J., Ridolfi, M., Sembhi, H., Sgheri, L., and Zoppetti, N.: Level 2 processor and auxiliary data for ESA Version 8 final full mission analysis of MIPAS measurements on ENVISAT, Atmospheric Measurement Techniques, 15, 1871–1901, https://doi.org/10.5194/amt-15-1871-2022, 2022.

Ravishankara, A. R., Daniel, J. S., and Portmann, R. W.: Nitrous Oxide (N_2O): The Dominant Ozone-Depleting Substance Emitted in the 21st Century, Science, 326, 123–125, https://doi.org/10.1126/science.1176985, 2009.

Ridolfi, M., Carli, B., Carlotti, M., von Clarmann, T., Dinelli, B. M., Dudhia, A., Flaud, J.-M., Höpfner, M., Morris, P. E., Raspollini, P., Stiller, G., and Wells, R. J.: Optimized forward model and retrieval scheme for MIPAS near-real-time dataprocessing, Applied Optics, 39, 1323–1340, https://doi.org/10.1364/AO.39.001323, 2000.

Riese, M., Tie, X., Brasseur, G., and Offermann, D.: Three-dimensional simulation of stratospheric trace gas distributions measured by CRISTA, Journal of Geophysical Research: Atmospheres, 104, 16 419–16 435, https://doi.org/10.1029/1999JD900178, 1999.

Roche, A. E., Kumer, J. B., Mergenthaler, J. L., Ely, G. A., Uplinger, W. G., Potter, J. F., James, T. C., and Sterritt, L. W.: The cryogenic limb array etalon spectrometer (CLAES) on UARS: Experiment description and performance, Journal of Geophysical Research: Atmospheres, 98, 10 763–10 775, https://doi.org/10.1029/93JD00800, 1993.

Semeniuk, K., McConnell, J. C., Jin, J. J., Jarosz, J. R., Boone, C. D., and Bernath, P. F.: N_2O production by high energy auroral electron precipitation, Journal of Geophysical Research: Atmospheres, 113, D16302, https://doi.org/10.1029/2007JD009690, 2008.

Sheese, P. E., Boone, C. D., and Walker, K. A.: Detecting physically unrealistic outliers in ACE-FTS atmospheric measurements, Atmospheric Measurement Techniques, 8, 741–750, https://doi.org/10.5194/amt-8-741-2015, 2015.

Sheese, P. E., Walker, K. A., Boone, C. D., Bernath, P. F., and Funke, B.: Nitrous oxide in the atmosphere: First measurements of a lower thermospheric source, Geophysical Research Letters, 43, 2866–2872, https://doi.org/10.1002/2015GL067353, 2016.

SPARC: SPARC CCMVal Report on the Evaluation of Chemistry-Climate Models, Tech. rep., SPARC, http://www.sparc-climate.org/publications/sparc-reports/, accessed on 21 October 2025, 2010.

SPARC: The SPARC Data Initiative: Assessment of stratospheric trace gas and aerosol climatologies from satellite limb sounders, Tech. rep., SPARC, http://www.sparc-climate.org/publications/sparc-reports/, accessed on 29 January 2025, 2017.

Strahan, S. and Douglass, A.: Evaluating the credibility of transport processes in simulations of ozone recovery using the Global Modeling Initiative three-dimensional model, Journal of Geophysical Research, 109, 27 545–27 564, https://doi.org/10.1029/2003JD004238, 2004.

Taylor, F. W., Rodgers, C. D., Whitney, J. G., Werrett, S. T., Barnett, J. J., Peskett, G. D., Venters, P., Ballard, J., Palmer, C. W. P., Knight, R. J., Morris, P., Nightingale, T., and Dudhia, A.: Remote sensing of atmospheric structure and composition by pressure modulator radiometry from space: The ISAMS experiment on UARS, Journal of Geophysical Research: Atmospheres, 98, 10 799–10 814, https://doi.org/10.1029/92JD03029, 1993.

Tian, H., Xu, R., Canadell, J. G., Thompson, R. L., Winiwarter, W., Suntharalingam, P., Davidson, E. A., Ciais, P., Jackson, R. B., Janssens-Maenhout, G., Prather, M. J., Regnier, P., Pan, N., Pan, S., Peters, G. P., Shi, H., Tubiello, F. N., Zaehle, S., Zhou, F., Arneth, A., Battaglia, G., Berthet, S., Bopp, L., Bouwman, A. F., Buitenhuis, E. T., Chang, J., Chipperfield, M. P., Dangal, S. R. S., Dlugokencky, E., Elkins, J. W., Eyre, B. D., Fu, B., Hall, B., Ito, A., Joos, F., Krummel, P. B., Landolfi, A., Laruelle, G. G., Lauerwald, R., Li, W., Lienert, S., Maavara, T., MacLeod, M., Millet, D. B., Olin, S., Patra, P. K., Prinn, R. G., Raymond, P. A., Ruiz, D. J., van der Werf, G. R., Vuichard,

https://doi.org/10.5194/egusphere-2026-4651
Preprint. Discussion started: 18 August 2026

N., Wang, J., Weiss, R. F., Wells, K. C., Wilson, C., Yang, J., and Yao, Y.: A comprehensive quantification of global nitrous oxide sources and sinks, Nature, 586, 248–256, https://doi.org/10.1038/s41586-020-2780-0, 2020.

Toon, G. C.: The JPL MkIV interferometer, Optica and Photonics News, 2, 19–21, https://doi.org/10.1364/OPN.2.10.000019, 1991.

Urban, J., Lautié, N., Le Flochmoën, E., Jiménez, C., Eriksson, P., de La Noë, J., Dupuy, E., Ekström, M., El Amraoui, L., Frisk, U., Murtagh, D., Olberg, M., and Ricaud, P.: Odin/SMR limb observations of stratospheric trace gases: Level 2 processing of ClO, N_2O, HNO_3, and O_3, Journal of Geophysical Research: Atmospheres, 110, D14307, https://doi.org/10.1029/2004JD005741, 2005.

von Clarmann, T., Glatthor, N., Grabowski, U., Höpfner, M., Kellmann, S., Kiefer, M., Linden, A., Tsidu, G. M., Milz, M., Steck, T., Stiller, G. P., Wang, D. Y., Fischer, H., Funke, B., Gil-López, S., and López-Puertas, M.: Retrieval of temperature and tangent altitude pointing from limb emission spectra recorded from space by the Michelson Interferometer for Passive Atmospheric Sounding (MIPAS), Journal of Geophysical Research: Atmospheres, 108, 4746, https://doi.org/10.1029/2003JD003602, 2003.

von Clarmann, T., Höpfner, M., Kellmann, S., Linden, A., Chauhan, S., Funke, B., Grabowski, U., Glatthor, N., Kiefer, M., Schieferdecker, T., Stiller, G. P., and Versick, S.: Retrieval of temperature, H_2O, O_3, HNO_3, CH_4, N_2O, $ClONO_2$ and ClO from MIPAS reduced resolution nominal mode limb emission measurements, Atmospheric Measurement Techniques, 2, 159–175, https://doi.org/10.5194/amt-2-159-2009, 2009.

Waters, J., Froidevaux, L., Harwood, R., Jarnot, R., Pickett, H., Read, W., Siegel, P., Cofield, R., Filipiak, M., Flower, D., Holden, J., Lau, G., Livesey, N., Manney, G., Pumphrey, H., Santee, M., Wu, D., Cuddy, D., Lay, R., Loo, M., Perun, V., Schwartz, M., Stek, P., Thurstans, R., Boyles, M., Chandra, K., Chavez, M., Chen, G.-S., Chudasama, B., Dodge, R., Fuller, R., Girard, M., Jiang, J., Jiang, Y., Knosp, B., LaBelle, R., Lam, J., Lee, K., Miller, D., Oswald, J., Patel, N., Pukala, D., Quintero, O., Scaff, D., Van Snyder, W., Tope, M., Wagner, P., and Walch, M.: The Earth observing system microwave limb sounder (EOS MLS) on the Aura Satellite, IEEE Transactions on Geoscience and Remote Sensing, 44, 1075–1092, https://doi.org/10.1109/TGRS.2006.873771, 2006.

Wetzel, G. and Johansson, S.: GLORIA HEMERA-2022 Level2, https://doi.org/10.35097/t2hqj3ef41x9nb55, accessed 15 July 2026, 2025a.

Wetzel, G. and Johansson, S.: GLORIA HEMERA-2021 Level2, https://doi.org/10.35097/08495ek0eja9q53z, accessed 15 July 2026, 2025b.

Wetzel, G., Oelhaf, H., Kirner, O., Ruhnke, R., Friedl-Vallon, F., Kleinert, A., Maucher, G., Fischer, H., Birk, M., Wagner, G., and Engel, A.: First remote sensing measurements of ClOOCl along with ClO and $ClONO_2$ in activated and deactivated Arctic vortex conditions using new ClOOCl IR absorption cross sections, Atmospheric Chemistry and Physics, 10, 931–945, https://doi.org/10.5194/acp-10-931-2010, 2010.

Wetzel, G., Höpfner, M., Oelhaf, H., Friedl-Vallon, F., Kleinert, A., Maucher, G., Sinnhuber, M., Abalichin, J., Dehn, A., and Raspollini, P.: Long-term validation of MIPAS ESA operational products using MIPAS-B measurements, Atmospheric Measurement Techniques, 15, 6669–6704, https://doi.org/10.5194/amt-15-6669-2022, 2022.

Wetzel, G., Kleinert, A., Johansson, S., Friedl-Vallon, F., Höpfner, M., Ungermann, J., Neubert, T., Catoire, V., Crevoisier, C., Engel, A., Gulde, T., Jacquet, P., Kirner, O., Kretschmer, E., Kulessa, T., Laube, J. C., Maucher, G., Nordmeyer, H., Piesch, C., Preusse, P., Retzlaff, M., Schardt, G., Schillings, J., Schneider, H., Schönfeld, A., Schuck, T., Woiwode, W., Riese, M., and Braesicke, P.: Intercomparison and validation of first GLORIA-B measurements of stratospheric and upper tropospheric long-lived tracers and photochemically active species, Atmospheric Measurement Techniques, 18, 5873–5894, https://doi.org/10.5194/amt-18-5873-2025, 2025.

https://doi.org/10.5194/egusphere-2026-4651
Preprint. Discussion started: 18 August 2026

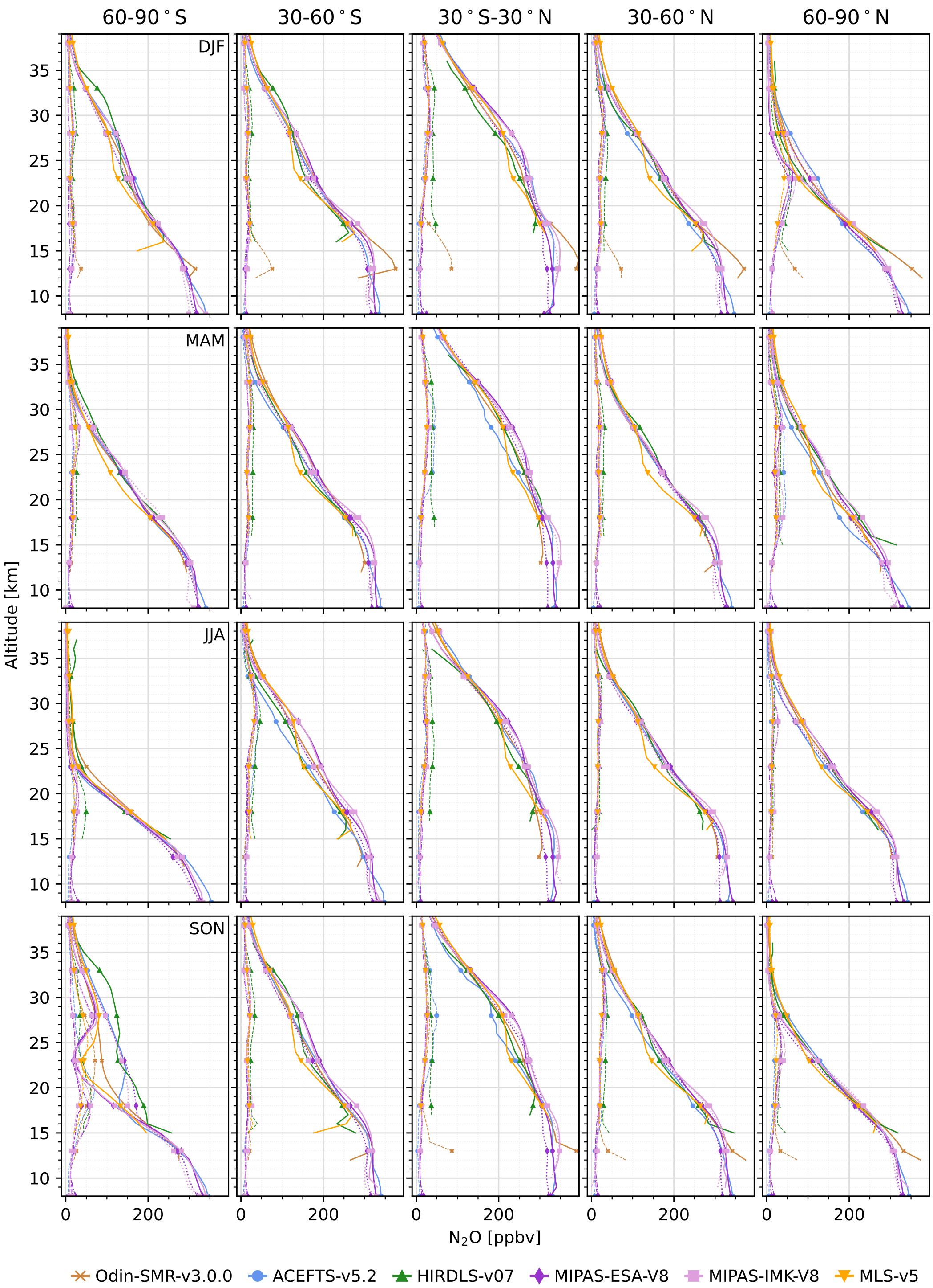

Figure 1. Median VMR (solid, except MIPAS full-resolution period, dotted) and median absolute deviation of the VMR (dashed, except MIPAS full-resolution period, dash-dotted) for each instrument, within different latitude bands (column) for each season (row). For SMR, all profiles were included in the median. For other instruments, only profiles coincident with an SMR profile were included. The MIPAS datasets are split into the full-resolution (dotted/dash-dotted) and reduced-resolution (solid/dashed) periods.

https://doi.org/10.5194/egusphere-2026-4651
Preprint. Discussion started: 18 August 2026

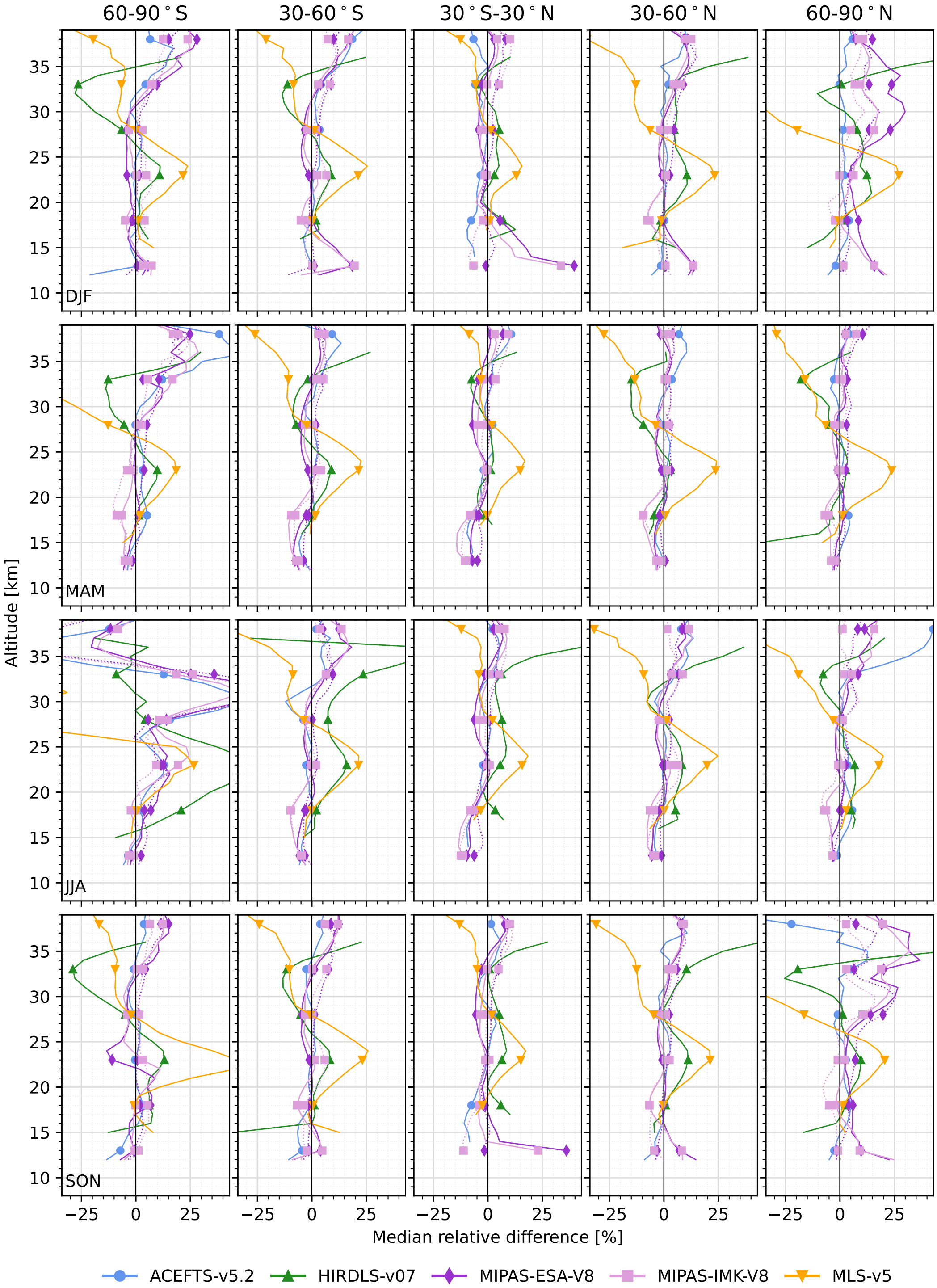

Figure 2. Median relative difference between SMR and coincident measurements from each other instrument, within each latitude band (column) for each season (row). The MIPAS datasets are split into the full-resolution (dotted) and reduced-resolution (solid) periods.

https://doi.org/10.5194/egusphere-2026-4651
Preprint. Discussion started: 18 August 2026

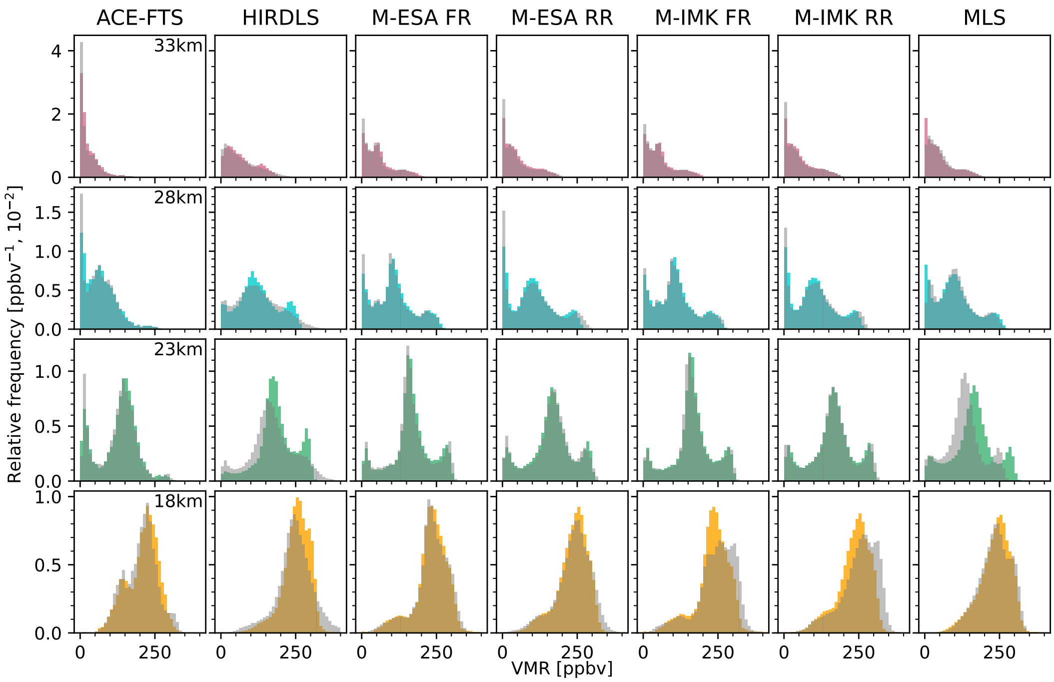

Figure 3. PDFs of SMR (coloured) N_2O measurements that are coincident with each other dataset (grey).

https://doi.org/10.5194/egusphere-2026-4651
Preprint. Discussion started: 18 August 2026

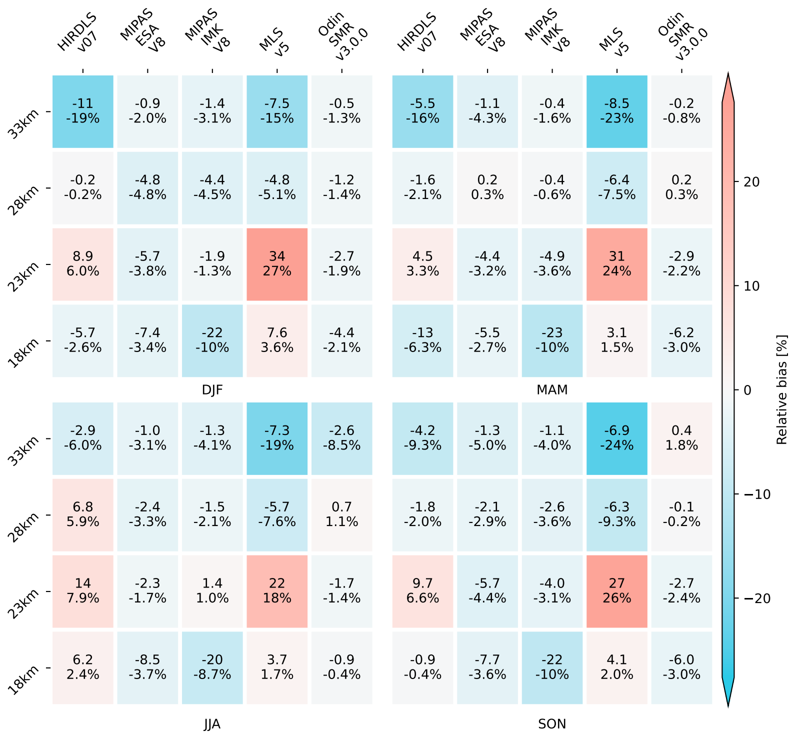

Figure 4. Median absolute N_2O bias (in ppbv) and relative bias between ACE-FTS and each other instrument at various altitudes during each season.

https://doi.org/10.5194/egusphere-2026-4651
Preprint. Discussion started: 18 August 2026

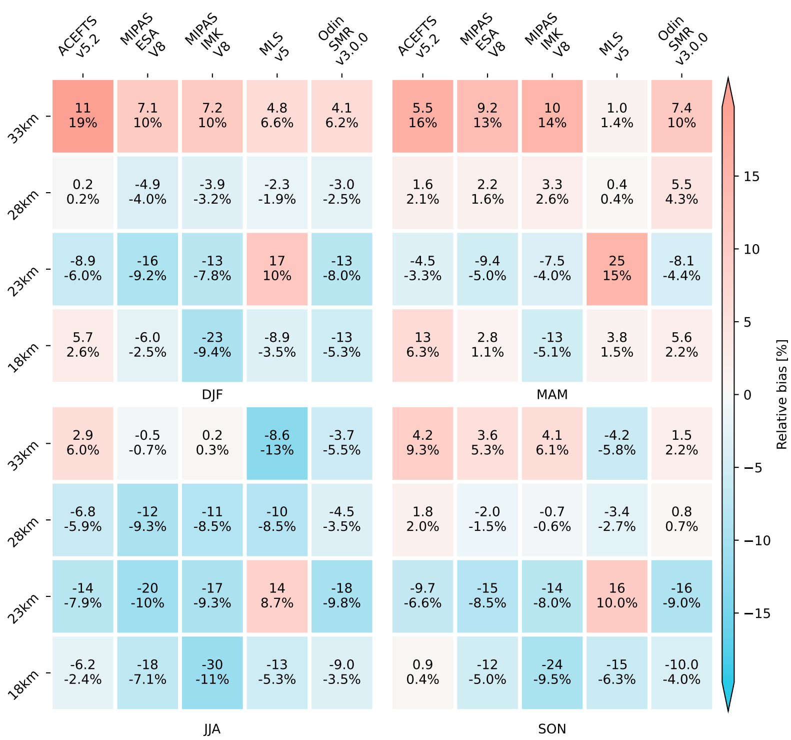

Figure 5. Median absolute N_2O bias (in ppbv) and relative bias between HIRDLS and each other instrument at various altitudes during each season.

https://doi.org/10.5194/egusphere-2026-4651
Preprint. Discussion started: 18 August 2026

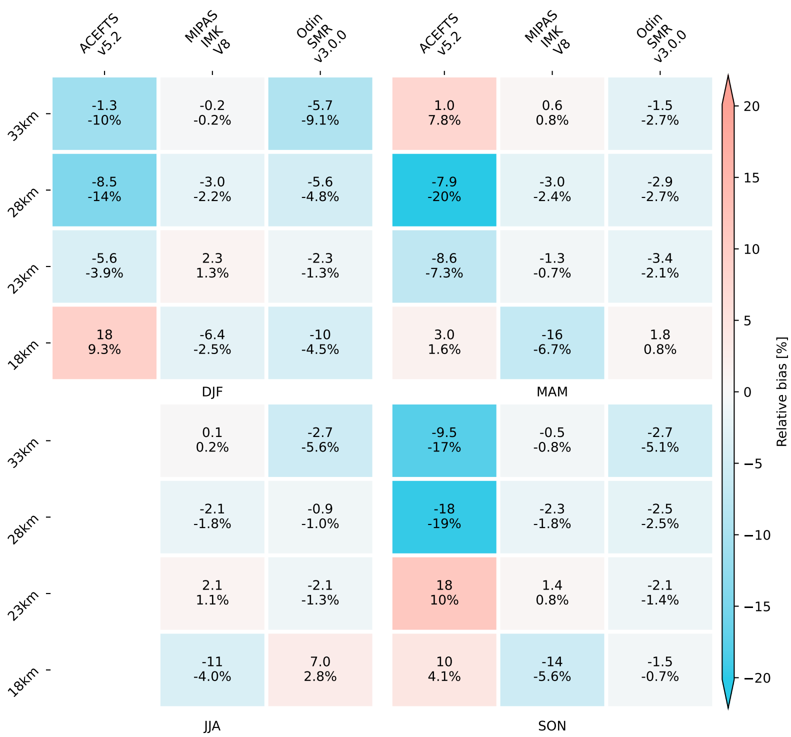

Figure 6. Median absolute N_2O bias (in ppbv) and relative bias between MIPAS-ESA FR and each other instrument at various altitudes during each season.

https://doi.org/10.5194/egusphere-2026-4651
Preprint. Discussion started: 18 August 2026

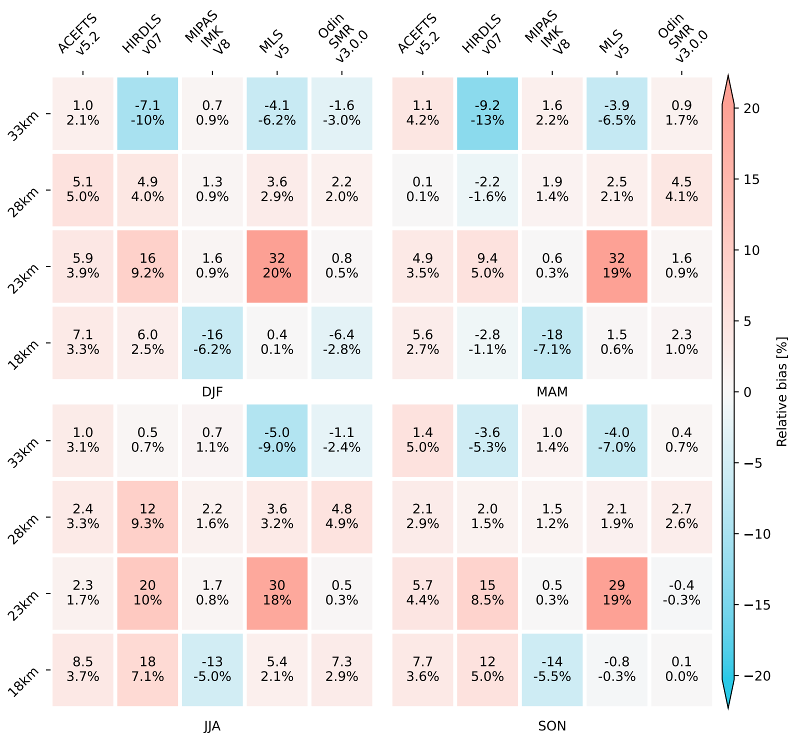

Figure 7. Median absolute N_2O bias (in ppbv) and relative bias between MIPAS-ESA RR and each other instrument at various altitudes during each season.

https://doi.org/10.5194/egusphere-2026-4651
Preprint. Discussion started: 18 August 2026

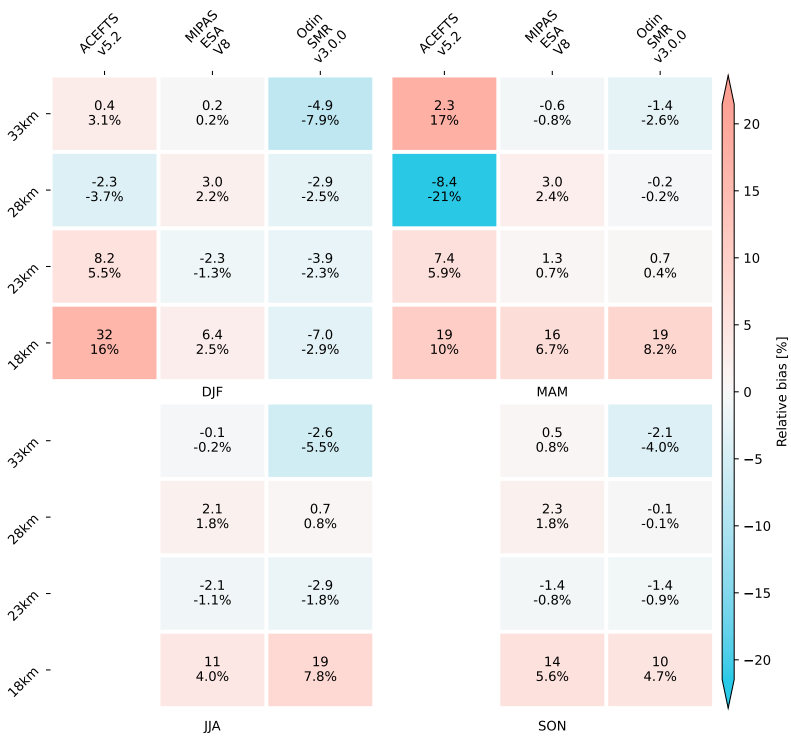

Figure 8. Median absolute N_2O bias (in ppbv) and relative bias between full-resolution MIPAS-IMK and each other instrument at various altitudes during each season.

https://doi.org/10.5194/egusphere-2026-4651
Preprint. Discussion started: 18 August 2026

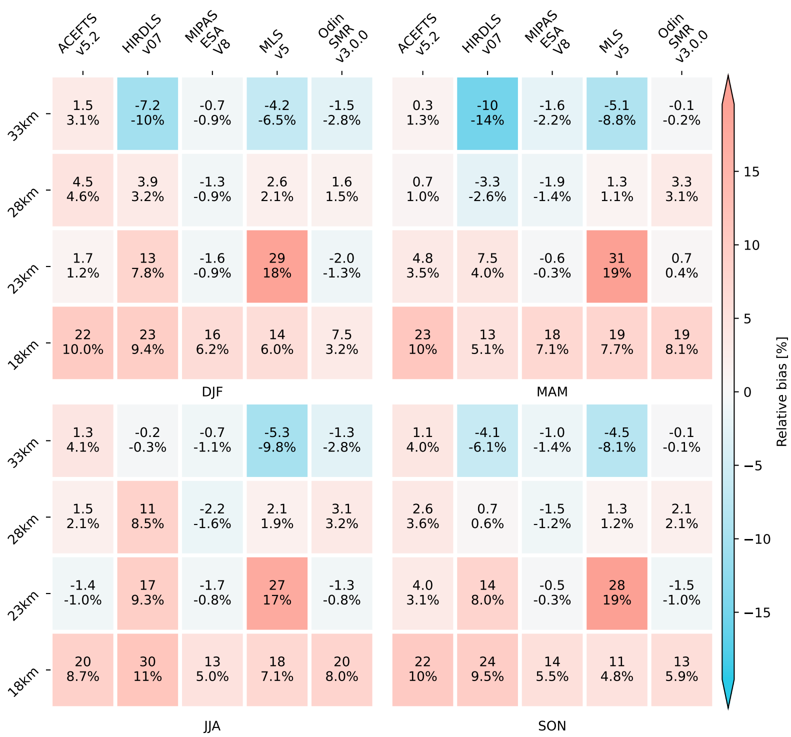

Figure 9. Median absolute N_2O bias (in ppbv) and relative bias between reduced-resolution MIPAS-IMK and each other instrument at various altitudes during each season.

https://doi.org/10.5194/egusphere-2026-4651
Preprint. Discussion started: 18 August 2026

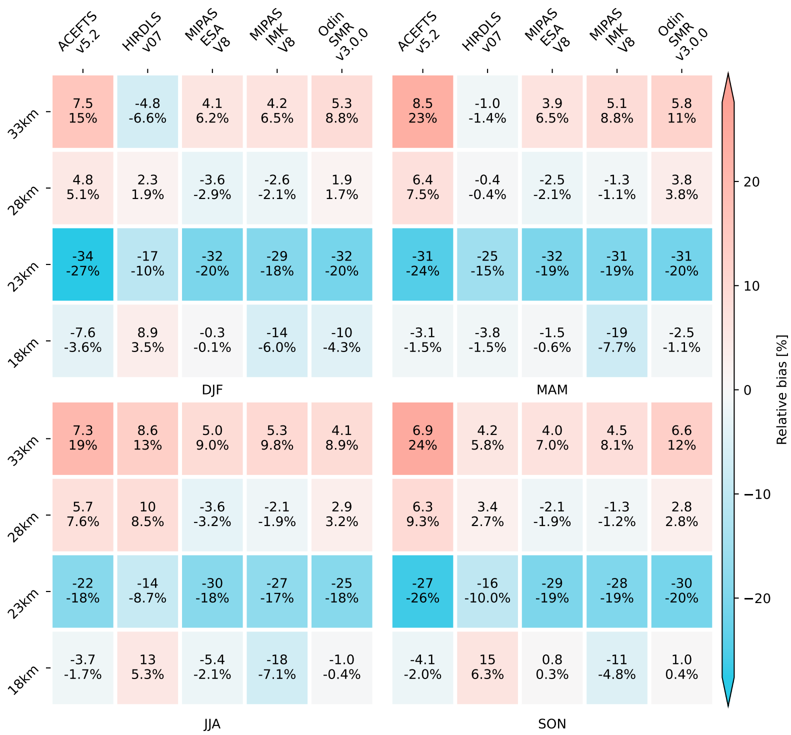

Figure 10. Median absolute N_2O bias (in ppbv) and relative bias between MLS v5 and each other instrument at various altitudes during each season.

https://doi.org/10.5194/egusphere-2026-4651
Preprint. Discussion started: 18 August 2026

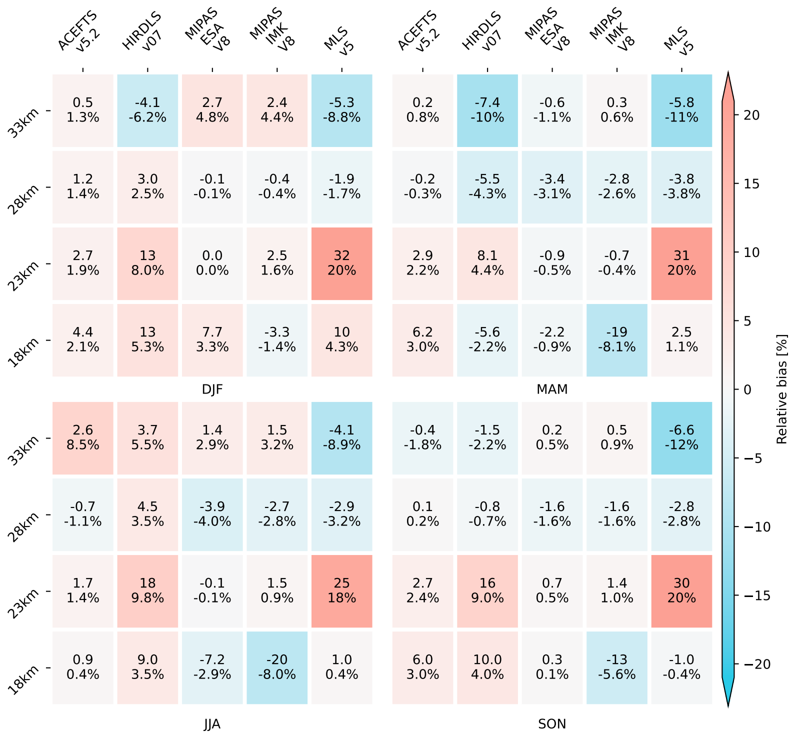

Figure 11. Median absolute N_2O bias (in ppbv) and relative bias between SMR and each other instrument at various altitudes during each season.

https://doi.org/10.5194/egusphere-2026-4651
Preprint. Discussion started: 18 August 2026

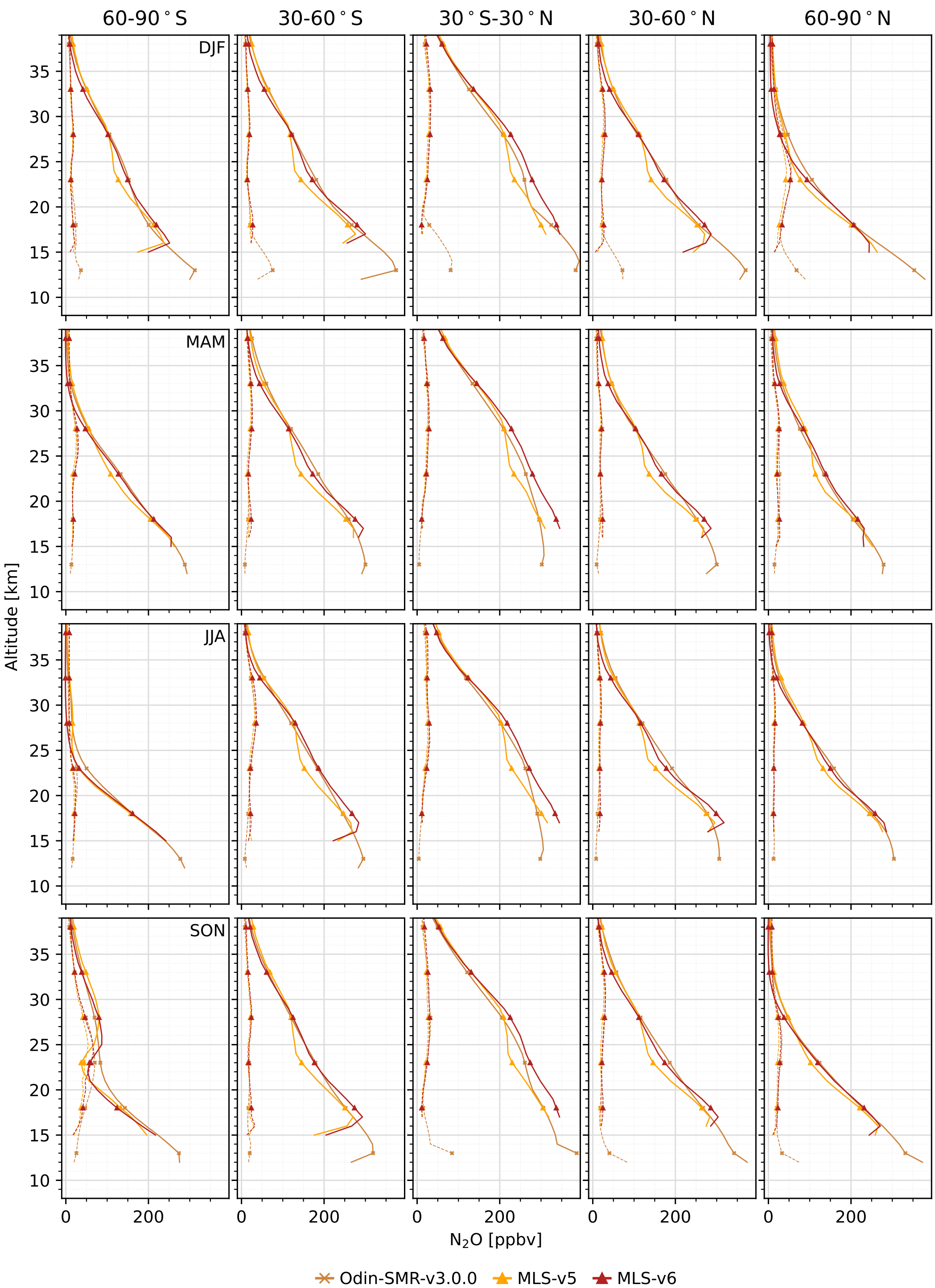

Figure 12. Median VMR (solid) and median absolute deviation of the VMR (dashed) for MLS v5 and v6 profiles that are coincident with SMR.

https://doi.org/10.5194/egusphere-2026-4651
Preprint. Discussion started: 18 August 2026

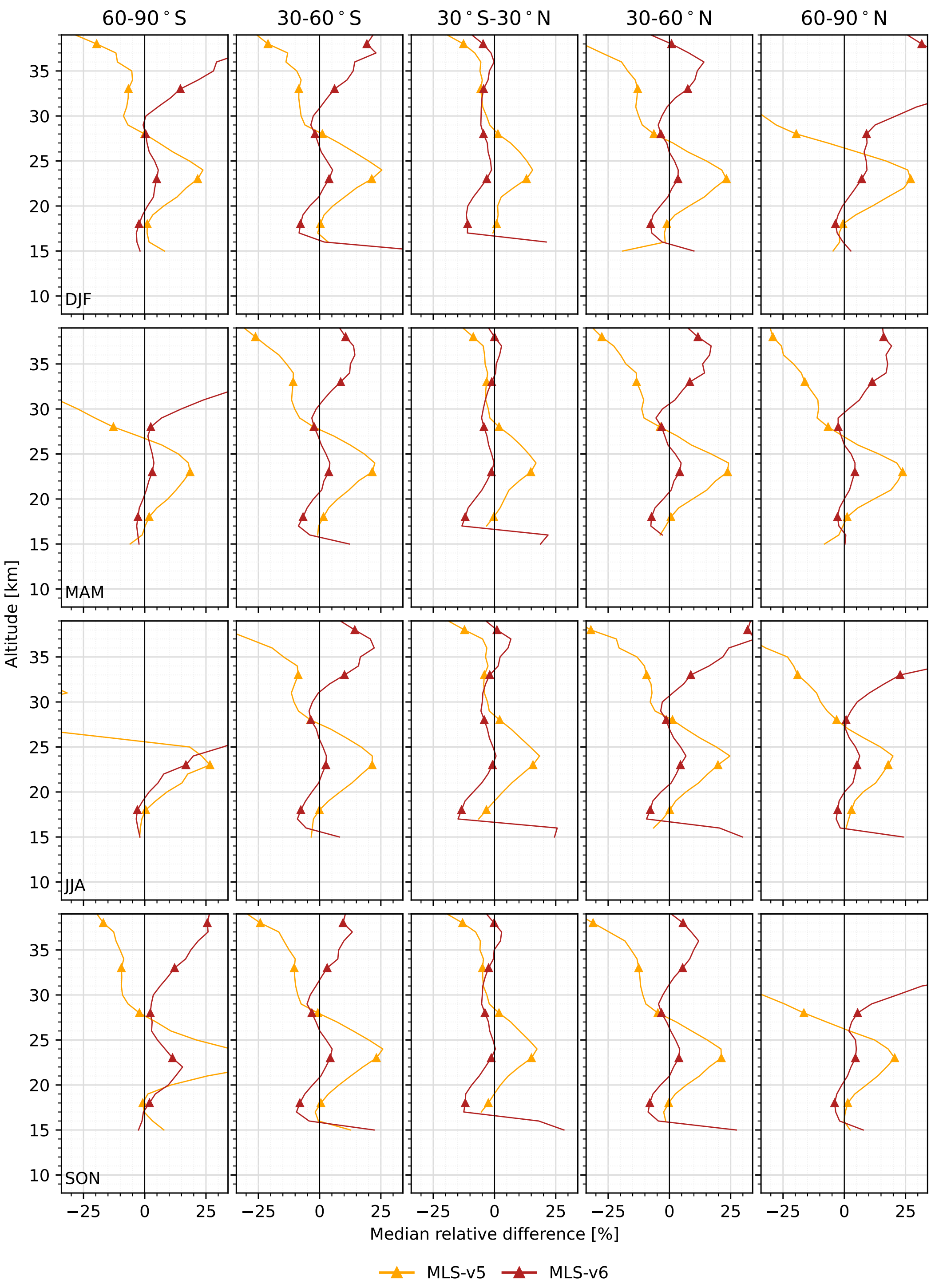

Figure 13. Median relative difference between SMR and coincident measurements from MLS v5 and MLS v6, within each latitude band (column) for each season (row).

https://doi.org/10.5194/egusphere-2026-4651
Preprint. Discussion started: 18 August 2026

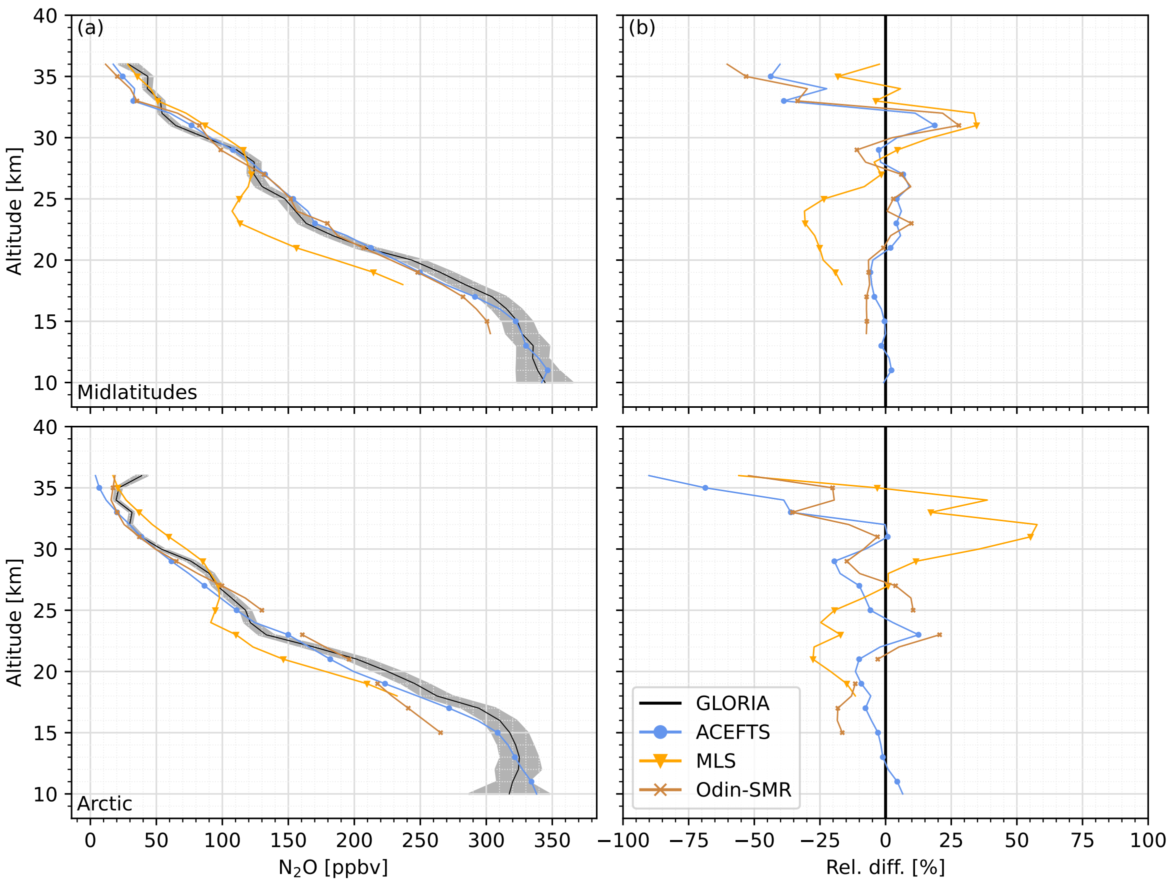

Figure 14. (a) Mean GLORIA-B N_2O profiles (black, see Section 4.1 for details about the calculation) compared with mean ACE-FTS (blue), MLS v5 (orange), and SMR (brown) profiles in the midlatitudes (top) and the Arctic (bottom). Grey shading represents the reported uncertainty of the GLORIA-B profiles. (b) Relative difference between each mean satellite profile and the mean GLORIA-B profile ((satellite−balloon)/balloon) in the midlatitudes (top) and the Arctic (bottom).

https://doi.org/10.5194/egusphere-2026-4651
Preprint. Discussion started: 18 August 2026

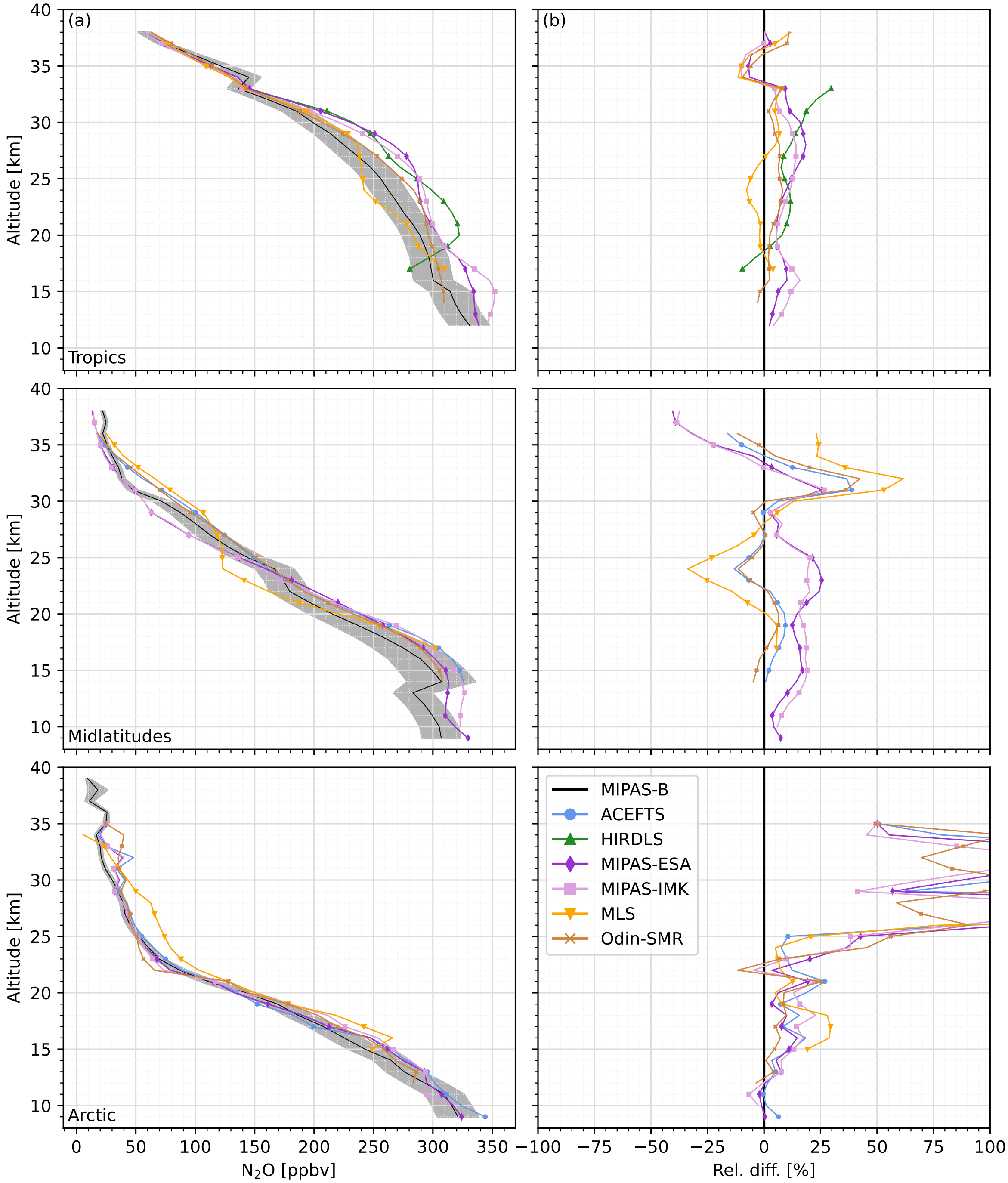

Figure 15. Same as Figure 14 but with MIPAS-B as the reference and including comparisons with HIRDLS (green), MIPAS-ESA (purple), and MIPAS-IMK (pink). An additional row is added at the top to show comparisons in the tropics.

https://doi.org/10.5194/egusphere-2026-4651
Preprint. Discussion started: 18 August 2026

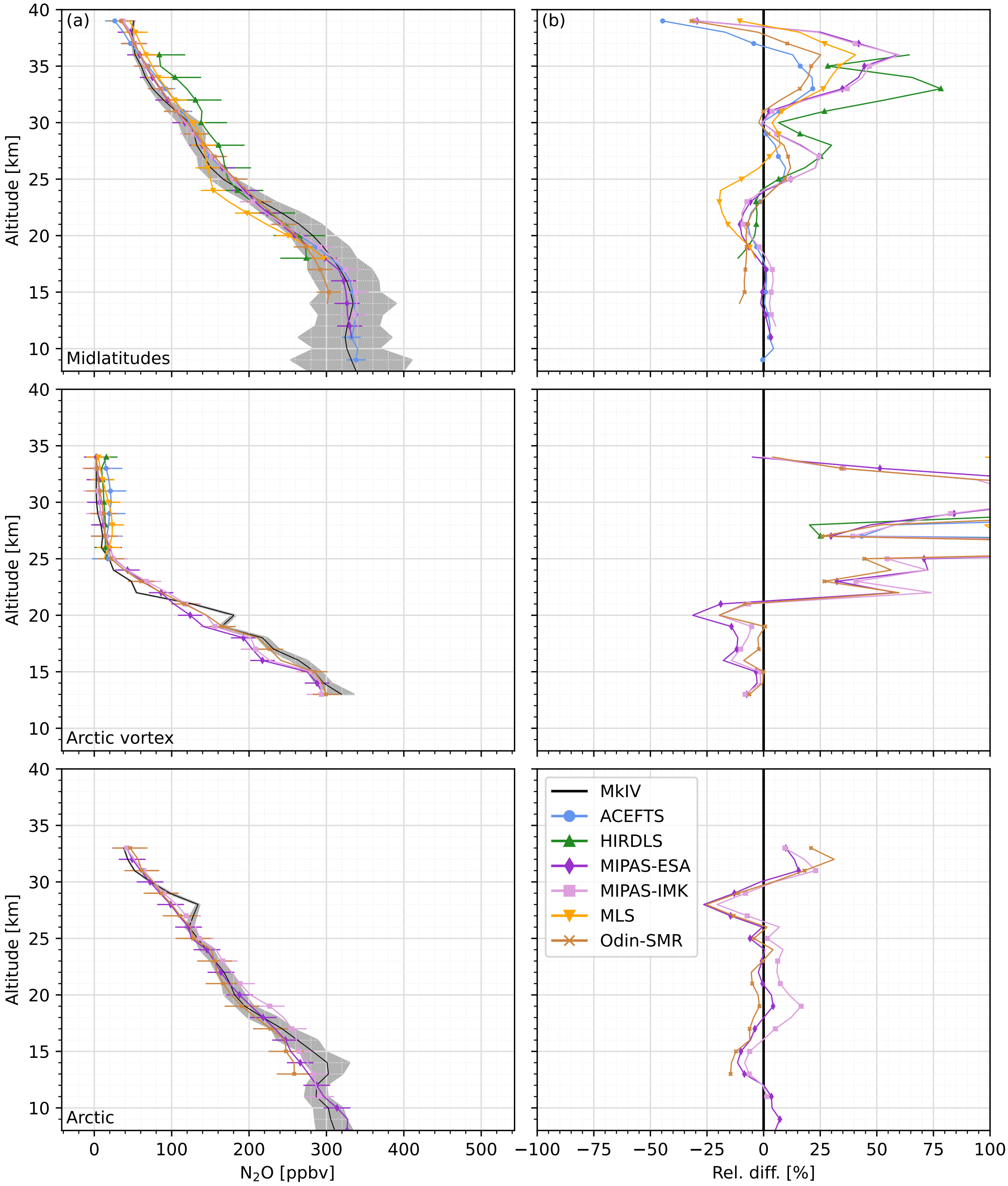

Figure 16. Same as Figure 15 but with MkIV as the reference, without comparisons in the tropics, and with the Arctic comparison separated into vortex (middle) and extravortex (bottom).

https://doi.org/10.5194/egusphere-2026-4651
Preprint. Discussion started: 18 August 2026

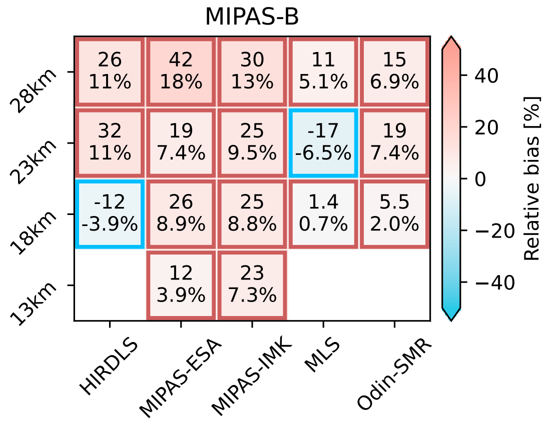

Figure 17. Summary of N_2O comparisons in the tropics. Absolute differences are shown in ppbv above the relative differences. Coloured borders indicate where the magnitude of the relative difference is less than 50%.

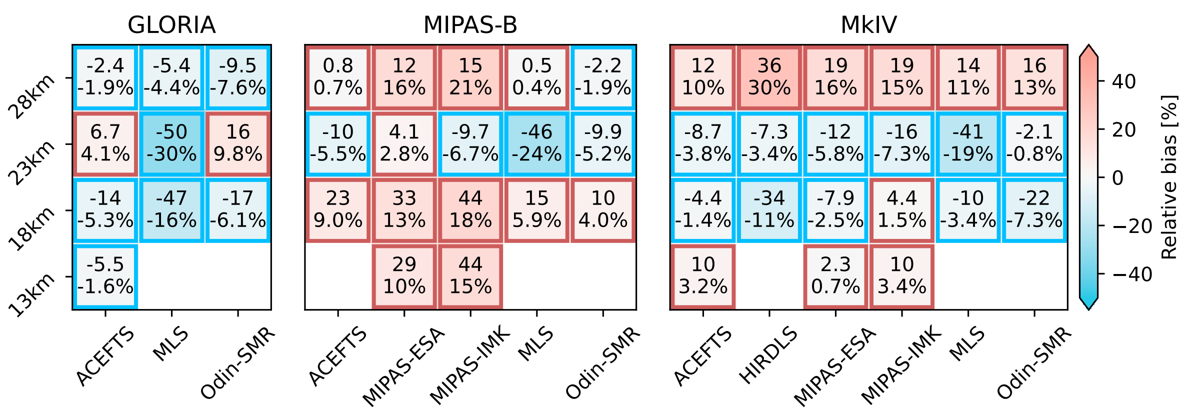

Figure 18. Same as Figure 17 but for the midlatitudes.

https://doi.org/10.5194/egusphere-2026-4651
Preprint. Discussion started: 18 August 2026

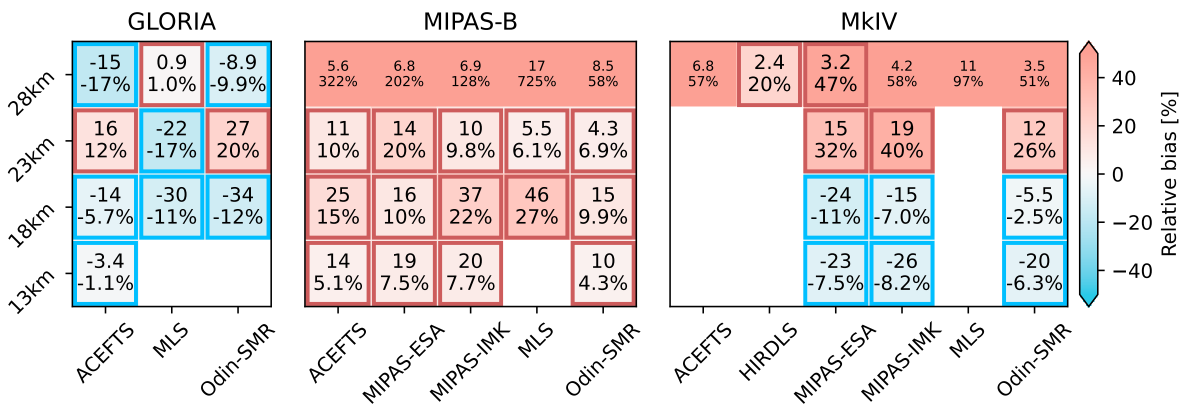

Figure 19. Same as Figure 17 but for the Arctic.